e−π Separation in the Barrel Electromagnetic Calorimeter with 2002 Test Beam Data

Liang Lu, Yongsheng Gao, Ryszard Stroynowski

Southern Methodist University
Dallas, TX 75275-0175, USA

October 9, 2003

Abstract

We study the separation of the electron and pion signals in the barrel electromagnetic calorimeter using the data from the test beam exposure of Module P15 to the electrons and pions in the momentum range from 20 to 180 GeV/c. Result using both simple cut and Neural Network methods are presented. We find that the spread of the shower through the layers of LARG described as the number of hit cells in these layers provide significant additional discriminative power. The study shows a good e−π separation capability in the whole momentum range. Using information from the LARG only and allowing 90% electron identification efficiency, we can achieve pion fake rate of $(1.8 − 3.2)\%$ with simple cuts. Assuming track momentum is well measured, the pion fake rates can be reduced to $(0.03 − 0.5)\%$ while maintaining 90% electron identification efficiency. Further significant improvements can be obtained by using Neural Network analysis method.

1   Introduction

Excellent particle identification is one of the most important design criteria for the ATLAS experiment [1]. ATLAS electromagnetic calorimeter is designed to identify photons and electrons in a wide energy range. Good electron identification and e−π separation capability is especially important in the momentum range below 200 GeV/c. In that momentum range one expects a large number of pions to be produced in the proton-proton collisions at 14 TeV. The electromagnetic shower generated by the electrons is expected to be fully contained in the calorimeter. The hadronic shower is expected to leak at the back of the calorimeter module into the hadronic calorimeter. However, a fraction of the hadronic showers may be fully contained within the calorimeter creating a potential for particle misidentification. In this note we use the longitudinal and lateral segmentations of the calorimeter to minimize the pion misidentification as electrons while maintaining high electron identification efficiency. Both simple cut and Neural Network methods are used for this e−π separation study with all beam momenta.

2 Data

The data were obtained during June and July 2002 in the exposure of the electromagnetic barrel module P15 to the test beam in the CERN North Area. The H8 beam line provided the electron and pion beams at the momenta of 20, 40, 100, 120, 150 and 180 GeV/c. The beam impinged on the calorimeter at fixed incident angle and position corresponding to $\eta = 11$ and $\phi = 40$.

The beam available in the H8 area is either a secondary or tertiary particle beam tuned for the energy and particle content. A 450 GeV/c primary proton beam is extracted from the SPS toward the North Areas and directed onto the primary target. The magnets located after the primary target provide the momentum selection for the secondary beam that contains mostly pions. Electrons are obtained in the tertiary beams. None of the beams available during the test-beam runs were pure. The fractions of electrons and pions (or kaons) in the beam varied with beam setting. In addition, pion decays in flight provided an admixture of muons.

The test beam setup is shown in Fig. 1. In front of the cryostat with the calorimeter module, there are four wire chambers and four scintillation counters that provide trigger information and determine the direction of the incoming particles. Additional scintillation counters, separated by an iron absorber, are located after the cryostat. Signals from these scintillators are used to identify and veto muons in the beam. In addition, one of the two pressure gas Cerenkov counters located in the beam line is filled with Helium gas. Its signals allow for the electron-pion separation for beam momenta up to about 80 GeV/c. The summary of test beam data is given in Table 1.

The standard single beam particle trigger and the standard data acquisition system is used in data collection. The Data Acquisition System used in the test beam setup is described in [2]. The data are collected in an asynchronous mode, i.e., beam particles arrived at random times during the accelerator spill but the calorimeter signals are sampled at a fixed frequency generated by the 40.08 MHz clock. Typically, in each run, about 10% of the events are due to random triggers.

To extract the signals and calculate energy deposited in each calorimeter cell we use the EMTB software [3] with the Optimal Filtering coefficients [4]. We then use the "sliding window" method [5] to reconstruct the clusters of cells and to find the total energy deposited in a cluster. For each calorimeter readout channel the pedestals are evaluated from the dedicated calibration run 217578 with 2,000 events collected at high and medium gains. For each cell, the optimal filtering coefficients are calculated using the calibration run data.

2.1 Clustering and Energies in Layers

The calorimeter is built in a projective geometry. The calorimeter modules are divided into the readout cells as illustrated in Fig. 2. The angular acceptance of each cell varies among the calorimeter layers as listed in Table 2.

A "sliding window" method [5] is used to find the position of a cluster of cells with the maximum energy deposit in a given layer. In most of the cases, the energy deposited by an electromagnetic shower is distributed over several cells in each layer. The cluster size is described by the number of cells in η and ϕ that contain most of the shower in layer 2. We select a cluster of cells using a standard EMTB method and take a cluster size of 3x3 cells in

2

Table 1: The summary of test beam data events, beam energies and the dominant beam content for each run.

E (GeV)	Nominal Beam	Run Number	No. of events
20	e	217630, 217631	25343
20	π	217628	11631
40	e	217623	27255
40	π	217587, 217588 217627	33941
100	e	217620	39997
100	π	217619	19998
120	e	217581, 217608	49970
120	π	217582, 217583 217618, 217635 217636, 217638	108422
150	e	217607, 217617	29443
150	π	217604, 217605	49482
180	e	217593, 217594 217595, 217596	83001
180	π	217569, 217570 217571, 217572 217573, 217580 217602	107584

the middle layer (layer 2) of the calorimeter. We sum the energies of the 3x3 cells centered around the cell with the largest energy deposit to obtain the energy deposited in the layer 2.

Because the cell geometry are different among the layers, such cluster selection in layer 2 corresponds to clusters consisting of 3x1 cells in the presampler, 24x1 cells in layer 1 and 2x3 cells in layer 3. The total energy deposited by an electron is reconstructed by summing the calibrated energies deposited in the presampler and in the three calorimeter layers. Previous studies indicate that the choice of the 3x3 cells window in the middle layer is sufficient to contain about 90% of the total energy deposited in the calorimeter [6]. In each layer, the cluster position is calculated as the energy weighted barycenter.

To correct for the energy loss upstream of the calorimeter, mainly due to the cryostat walls, the energy deposited in the presampler is weighted by a factor α when calculating the total energy deposited ($E_{Cluster}$). Longitudinal energy leakage induces a deterioration of the energy resolution, therefore a weight β is also applied to the energy deposited in the back compartment:

$$E_{Cluster} = \alpha E_{Presampler} + E_{Layer1} + E_{Layer2} + \beta E_{Layer3}$$

The parameters α and β are obtained by minimizing the energy resolution for each η position.

Cherenkov counter in the testbeam setup is filled with Helium gas at a pressure of 10^{-1} bar. The momentum threshold for a pion to generate the Cherenkov light was about 80 GeV/c.

Table 2: Angular acceptance of cells in the barrel calorimeter.

Calorimeter layer	$\Delta\eta$	$\Delta\phi$
Presampler	0.025	0.1
Layer 1	0.003	0.1
Layer 2	0.025	0.025
Layer 3	0.050	0.025

Therefore, the counter provides an independent and efficient tag of electrons and pions for the beam momenta of 20 and 40 GeV/c. The ADC distributions of the Cherenkov signals are shown in Fig. 3 for the nominal electron and pion beams of 20GeV. We require ADC counts from Cherenkov counter to be greater than 400 to select our electron sample.

We require Cherenkov ADC counts to be less than 400 for the pion run data to select our pion samples at all momenta. An additional muon veto is applied to remove muons for both electron and pion sample selection.

Since the Cherenkov detector can not separate electrons from pions when momenta of the beam are above 80GeV/c, we cut on the $E_{cluster}$ to select electron samples for 100GeV or higher. Table 3 lists the corresponding cuts to select the electron samples for higher energies. We will discuss how these cut values are determined in the later section.

Table 3: The cuts on $E_{cluster}$ to select electron samples of 100GeV, 120GeV, 150GeV and 180GeV.

Beam Momentum (GeV)	Cut on $E_{cluster}$
100	$E_{total} > 89.5$ GeV
120	$E_{total} > 108.5$ GeV
150	$E_{total} > 136.5$ GeV
180	$E_{total} > 170.5$ GeV

The distributions of the energy deposited in each layer as well as the distribution of the total energy in the calorimeter are shown in Fig. 4 for the electron and pion samples at 20 GeV/c beam energy and the 40 GeV/c beams. The 100 GeV/c beam energy and the 120 GeV/c beams plots are shown in Fig. 5. The 150 GeV/c beam energy and the 180 GeV/c beams plots are shown in Fig. 6.

2.2 The Lateral Profile: Number of Hit Cells

The shape of the longitudinal profile of the shower is contained in the information of the energy deposited in each layer of the calorimeter. Additional information is contained in the lateral shower profile characterized by the number of "hit" cells in each layer, i.e., the number of cells that contain energy above the noise level (pedestal). The noise level for each layer is obtained

using the random trigger. The corresponding energy distribution in selected cells are shown in Fig. 7.

We fit the noise distribution with Gaussian function and the noise level is give by the standard deviations (σ) of the fitting result. We find that all cells in a given layer of the calorimeter have very similar noise level. The corresponding noise levels are listed in Table 4 together with the minimum values of the energy required for a "hit" cell in the layers. They correspond to a cut of 5 (σ) above the noise level.

Table 4: The noise level of each layer and the definition of a "hit" cell, and the 5σ minimum energy required in the "hit" cell definition.

Calorimeter layer	Noise Level(GeV)	Requirement for a "hit" cell (GeV)
Presampler	0.044	0.220
Layer 1	0.012	0.060
Layer 2	0.032	0.160
Layer 3	0.021	0.105

In the subsequent analysis, we count the number of hit cells in a given layer only within the selected cluster. The number of hit cells for electrons and pions beams at various energies are shown in Fig. 8 for the 20 and 40 GeV/c beams, Figure $9 - 10$ for other energies. From these plots, we can see that the numbers of hit cells are quite different for electrons and pions and may provide additional discrimination power.

In general, the number of hit cells and the energy fraction in a given layer can be correlated. To check the correlation between the number of hits in a layer and the fraction energy deposited in that layer, we make 2 dimension plots Fig. $11 - 22$.

These distributions show that the correlations are weak and the number of hit cells in the layers will provide additional information that can result in the same selection efficiency for electrons with significantly better pion rejection.

3 Analysis Strategy

We study the electron identification and e$-\pi$ separation with LARG information only. In addition, we also perform the same study assume the momentum of the track is well measured.

3.1 Break down of the $e - \pi$ separation power

In order to have a better understanding of how useful the LARG information is in separating electrons and pions, We try to break down the e$-\pi$ separation due to various sets of information for all energies.

- **Using Longitudinal Profile only, i.e. the energy ratios.**

Instead of the energy deposits in each layer which depends on the absolute momentum of the track, we use the ratios of the energy in each individual layers to the total energy deposited

of all layers $E_{Cluster}$: $E_0/E_{Cluster}$ is the ratio of energy deposited in the presampler to the total energy, $E_1/E_{Cluster}$ is the ratio of energy deposited in the layer 1 to the total energy, $E_2/E_{Cluster}$ is the ratio of energy deposited in the layer 2 (middle) to total energy, $E_3/E_{Cluster}$ is the ratio of energy deposited in the layer 3 (back) to the total energy. To obtain the fraction of the energy deposited in the core of the shower we project the center cell of the shower in the middle layer onto the other layers and calculate the total energy deposited in the corresponding tower of the calorimeter. The fraction of the shower energy concentrated in the core is then $E_{11}/E_{Cluster}$.

The obvious advantage of using these energy ratios instead of the energy deposits in each layer is the less dependency to the absolute momentum of the track.

- **Using Longitudinal and Lateral (Number of Hit Cells) Profiles**

Beside the energy ratio, we also use the number of hit cells in each layer. NH(0) is the number of hit cells of presampler, NH(1) is the number of hit cells of layer 1, NH(2) is the number of hit cells of layer 2 and NH(3) is the number of hit cells of layer 3.

So far these information are from LARG only, no other information is used. The distributions of these variables together with the distributions of the number of hit cells in each layer are shown in Figs 23− 28.

- **Using Longitudinal, Lateral Profiles and** $E_{Cluster}/P$

P is the momentum of the beam in each run. Here we assume the momentum of the track is also measured, i.e. we are using additional information besides the information provided by LARG. We study e−π separation with electron and pion samples of the same momentum. This is only possible when the track momentum is measured.

3.2   Analysis Methods

The above variables are used in two analysis methods for e−π separation study. The first method is based on simple cuts on these variables. To exploit the best separation power from the detector information, we use the Neural Network approach as the second method with the same variables.

Neural Network approach has been widely used in high energy physics experiments. Some general introduction and an application in ATLAS can be found in [7].

We use the package of Multi-Layer Perceptron (MLP) program [8] to construct our neural network. We use Broyden-Fletcher-Goldfarb-Shanno (BFGS) method [8] as a training process with one hidden layer. We follow the rule of thumb that the number of hidden neurons is about twice the number of input variables. Since the number of inputs variables changes with the different strategies, the number of neurons we use for the energy ratio only, energy ratio plus hit cells, energy ratio plus hit cells plus $E_{Cluster}/P$ are 11, 17 and 18 respectively. We find our Neural Network results are very stable when changing the number of hidden neurons around these values. We also check the error of the output of the neural network, so there is no over-training of the process.

We divide each data sample of a specific momentum and particle type into three equal subsamples. These subsamples serve as training sample, verification sample and testing sample.

4 Analysis for 20 and 40 GeV Test Beam Data

4.1 Electron and π Sample Selection

We require ADC counts from Cherenkov counter to be greater than 400 to select our electron sample. The ADC distribution of the Cherenkov signals is shown in Fig.3 for the nominal electron and pion beams. We normalize the pion run sample to the electron run sample with ADC counts less than 400 according to their total area. The tail of ADC counts distribution of the pion sample above 400 gives the maximum contamination in the electron sample. The purity of the electron sample is defined as the number of electron sample with pion contamination subtracted over the number of electron sample. The purity of the 20GeV and 40GeV electron samples are above 99.9%.

We require Cherenkov ADC counts to be less than 400 for the pion run data to select our pion samples at all momenta. Similarly, we can determine the electron contamination in pion samples. The purity of pion samples are above 99.0% for all momenta.

4.2 e$-\pi$ Separation Using Simple Cut Method

The results based on sequential cuts applied to the 20GeV electron and pion samples are summarized in Table 5. The first set of cuts are applied only on the longitudinal profile (i.e. the energy ratios), followed by the set of cuts on lateral profile (i.e. the number of hit cells in the layers). The last cut is on $E_{Cluster}/$P. With various sets of cuts, we try to keep the resulted electron identification efficiency at about 90% so we can compare the pion fake rates to understand the improvements in e$-\pi$ separation power with additional information from the number of hit cells in the layers and track momentum measurements.

Table 5: The results for 20GeV using simple cuts on longitudinal profile, lateral profile, longitudinal and lateral profiles plus E$_{Cluster}/$P.

20 GeV Sample by Cherenkov: ADC (e > 400, π < 400)	Electron Sample (Efficiency)	Pion Sample (Fake Rate)
After Quality and Cherenkov:	13855	10389
$E_{Cluster} > 0$, $0 < E_0/E_{Cluster} < 0.2$, $E_{11}/E_{Cluster} > 0.5$ $0 < E_3/E_{Cluster} < 0.015$, $E_2/E_{Cluster} > 0.4$	12502 $(90.02\pm1.11)\%$	715 $(6.88\pm0.27)\%$
$E_{Cluster} > 0$, $0 < E_0/E_{Cluster} < 0.2$, $E_{11}/E_{Cluster} > 0.45$ $E_3/E_{Cluster} < 0.015$, $E_2/E_{Cluster} > 0.4$ $0.1 < E_1/E_{Cluster} < 0.45$, $NH(0) > 0$, $NH(2) > 3$	12392 $(89.44\pm1.11)\%$	330 $(3.18\pm0.18)\%$
Above Energy Ratio and Number of Hit Cell cuts $E_{Cluster}/20.0\text{GeV} > 0.70$	12284 $(88.66\pm1.10)\%$	52 $(0.50\pm0.07)\%$

The results based on sequential cuts applied to the 40GeV electron and pion samples are summarized in Table 6. The first 6 cuts are applied only on the energy ratios, followed by the cuts on number of hit cells. The last cut is on $E_{Cluster}/$P. With various sets of cuts, we try to keep the electron identification efficiency at about 90% so we can compare the pion fake rates

to understand the improvements in e$-\pi$ separation power with additional information from hit cells and momentum measurements.

Table 6: The results for 40GeV using simple cuts on longitudinal profile, lateral profile, longitudinal and lateral profiles plus $E_{Cluster}/$P.

40 GeV Sample by Cherenkov: ADC (e > 400, π < 400)	Electron Sample (Efficiency)	Pion Sample (Fake Rate)
After Quality and Cherenkov:	2817	29512
$E_{Cluster} > 0$, $0 < E_0/E_{Cluster} < 0.1$, $E_{11}/E_{Cluster} > 0.45$ $0 < E_3/E_{Cluster} < 0.015$, $E_2/E_{Cluster} > 0.55$ $0.1 < E_1/E_{Cluster} < 0.4$	2523 (89.56±2.45)%	1873 (6.35±0.15)%
$E_{Cluster} > 0$, $0 < E_0/E_{Cluster} < 0.15$, $E_{11}/E_{Cluster} > 0.45$ $0 < E_3/E_{Cluster} < 0.015$, $E_2/E_{Cluster} > 0.5$ $0.1 < E_1/E_{Cluster} < 0.4$, $NH(0) > 0$, $NH(2) > 4$	2534 (89.95±2.46)%	1258 (4.26±0.12)%
Above Energy Ratio and Number of Hit Cell cuts $E_{Cluster}/40.0$GeV > 0.80	2508 (89.03±2.44)%	112 (0.38±0.04)%

4.3   e$-\pi$ Separation Using Neural Network Method

We perform the same electron identification and e$-\pi$ separation study based on various sets of variables using Neural Network to compare with the results using simple cuts. The first set of 6 variables are the energy ratios, followed by the number of hit cells, then $E_{Cluster}/$P. The Neural Network outputs using these various sets of variables of 20GeV are shown in Figure 29. To compare with the results using simple cuts, We cut on the Neural Network output and try to keep the electron identification efficiency at about 90% to find the corresponding pion fake rates. The results for 20GeV and 40GeV and their comparison with simple cut method are summarized in Table 7 and 8 respectively.

Table 7: The results for 20GeV using Neural Network method and the comparison with simple cut method.

20 GeV with 90% Electron Efficiency	Fake Rate (CUT)	Fake Rate (NN)
Energy Ratio	(6.88±0.27)%	(4.07±0.29)%
Energy Ratio + Hit Cells	(3.18±0.18)%	(2.42±0.22)%
Ratio+Hit Cells+$E_{Cluster}/20GeV$	(0.50±0.07)%	(0.34±0.08)%

Comparing the results from Neural Network and simples cuts, We can see that with the exact same information, the results using Neural Network are significantly better than those from simple cuts. After $E_{Cluster}/$P information is used, the electron and pion samples are well separated by the Neutral Network. The cut on Neural Network output with 90% electron identification efficiency eliminates 99.6% of the pion sample, only a few pion events in the tail

Table 8: The results for 40GeV using Neural Network method and the comparison with simple cut method.

40 GeV with 90% Electron Efficiency	Fake Rate (CUT)	Fake Rate (NN)
Energy Ratio	$(6.35\pm0.15)\%$	$(3.52\pm0.14)\%$
Energy Ratio + Hit Cells	$(4.26\pm0.12)\%$	$(1.88\pm0.10)\%$
Ratio+Hit Cells+$E_{Cluster}/40GeV$	$(0.38\pm0.04)\%$	$(0.07\pm0.02)\%$

are left. With the excellent e$-\pi$ separation capability demonstrated in this note, we will need much larger pion samples in the next combined test beam data taking, if we want to investigate e$-\pi$ separation with better statistics or with more information than LARG and momentum measurement.

5 Analysis for 100, 120, 150 and 180GeV Test Beam Data

5.1 100,120,150 and 180 GeV e,π sample selection

For these momenta which are above the Cherenkov counter threshold, the Cherenkov information is no longer useful to help us identify pure electron samples. For these momenta range, we cut on $E_{cluster}$ to select our electron samples as described in Table 3. The Cut on $E_{cluster}$ certainly introduces bias for our electron separation. The following study show how we estimate this bias.

5.2 Study of Bias Using 20 and 40GeV Samples with Cherenkov Tagging and Various Cuts on $E_{Cluster}$.

To study the bias introduced by cut on $E_{Cluster}$ for electron sample selection, we compare the results from electron samples selected by Cherenkov tagging and by cut on $E_{Cluster}$. We vary the cuts on $E_{Cluster}$ over a wide range and compare the differences in electron identification efficiencies of these electron samples with the same pion fake rates.

Table 9, 10 and 11 shows the results for 20GeV with Cherenkov tagging and various cuts on $E_{Cluster}$. The difference in electron identification efficiency with the Cherenkov tagging sample reflects the effect of the bias introduced by cut on $E_{Cluster}$. Because the cut on $E_{Cluster}$ eliminates the more "π-like" electrons, the electron identification efficiency for electron sample selected by cut on $E_{Cluster}$ is $(4-5)\%$ higher than that of the unbiased electron sample with electron identification efficiency of 90%.

Table 12, 13 and 14 shows the results for 40GeV with Cherenkov tagging and various cuts on $E_{Cluster}$. They are very similar to the results of 20GeV. The bias introduced to the electron identification efficiency due to the cut on $E_{Cluster}$ is about 5%.

Our $e - \pi$ separation power depends on the purity of the selected electrons and pions. Using the energy cut to define the electrons will introduce two additional errors than using

Table 9: The results for 20GeV using longitudinal profile with Cherenkov tagging and various cuts on $E_{Cluster}$.

20 GeV Electron Samples Energy Ratios	Electron Sample (Fake Rate)	Pion Sample (Efficiency)
By Cherenkov:	$(6.88\pm0.27)\%$	$(90.02\pm1.11)\%$
$E_{Cluster} > 16.2GeV$:	$(6.87\pm0.27)\%$	$(93.31\pm0.98)\%$
$|E_{Cluster} - 18.8GeV| < 3.0GeV$:	$(6.87\pm0.27)\%$	$(93.24\pm0.97)\%$
$|E_{Cluster} - 18.8GeV| < 2.0GeV$:	$(6.87\pm0.27)\%$	$(93.41\pm0.99)\%$
$|E_{Cluster} - 18.8GeV| < 1.0GeV$:	$(6.87\pm0.27)\%$	$(93.84\pm1.06)\%$
$|E_{Cluster} - 18.8GeV| < 0.5GeV$:	$(6.87\pm0.27)\%$	$(94.09\pm1.31)\%$

Table 10: The results for 20GeV using longitudinal and lateral profiles with Cherenkov tagging and various cuts on $E_{Cluster}$.

20 GeV Electron Samples Energy Ratios + Hit Cells	Electron Sample (Fake Rate)	Pion Sample (Efficiency)
By Cherenkov:	$(3.18\pm0.18)\%$	$(89.44\pm1.11)\%$
$E_{Cluster} > 16.2GeV$:	$(3.18\pm0.18)\%$	$(92.50\pm0.97)\%$
$|E_{Cluster} - 18.8GeV| < 3.0GeV$:	$(3.18\pm0.18)\%$	$(92.41\pm0.97)\%$
$|E_{Cluster} - 18.8GeV| < 2.0GeV$:	$(3.18\pm0.18)\%$	$(92.65\pm0.98)\%$
$|E_{Cluster} - 18.8GeV| < 1.0GeV$:	$(3.18\pm0.18)\%$	$(92.90\pm1.06)\%$
$|E_{Cluster} - 18.8GeV| < 0.5GeV$:	$(3.18\pm0.18)\%$	$(93.01\pm1.30)\%$

Cherenkov signal to select electron events. The first one is the electron sample purity depends on the Energy cut. For example, in 120 GeV, the purity of electron sample is 99.0%, which will introduce 1.0% error in final result. Second, the bias of the energy cut. This bias also depends on the cut of the Energy. The tighter the cut we set, the higher the purity and we get bigger bias. We set the cut on $E_{Cluster}$ so that the error from the purity to be small but comparable to the error from the bias. We choose the valuses of $E_{Cluster}$ cut so the purity of the sample id about 99.0%.

5.3 e$-\pi$ Separation Using Simple Cut Method

The results based on sequential cuts applied to the 100GeV or higher electron and pion samples are summarized in Table $15 - 18$

5.4 e$-\pi$ Separation Using Neural Network Method

We perform the same electron identification and e$-\pi$ separation study based on various sets of variables using Neural Network to compare with the results using simple cuts. To compare with the results using simple cuts, We cut on the Neural Network output and try to keep the electron

Table 11: The results for 20GeV using longitudinal and lateral profiles plus $E_{Cluster}/$P with Cherenkov tagging and various cuts on $E_{Cluster}$.

20 GeV Electron Samples Ratios+Hit Cells+$E_{Cluster}/20GeV > 0.7$	Electron Sample (Fake Rate)	Pion Sample (Efficiency)
By Cherenkov:	(0.50±0.07)%	(88.66±1.10)%
$E_{Cluster} > 16.2GeV$:	(0.50±0.07)%	(92.50±0.97)%
$|E_{Cluster} - 18.8GeV| < 3.0GeV$:	(0.50±0.07)%	(92.41±0.97)%
$|E_{Cluster} - 18.8GeV| < 2.0GeV$:	(0.50±0.07)%	(92.65±0.98)%
$|E_{Cluster} - 18.8GeV| < 1.0GeV$:	(0.50±0.07)%	(92.90±1.06)%
$|E_{Cluster} - 18.8GeV| < 0.5GeV$:	(0.50±0.07)%	(93.01±1.30)%

Table 12: The results for 40GeV using longitudinal profile with Cherenkov tagging and various cuts on $E_{Cluster}$.

40 GeV Electron Samples Energy Ratios	Electron Sample (Fake Rate)	Pion Sample (Efficiency)
By Cherenkov:	(6.35±0.15)%	(89.56±2.45)%
$E_{Cluster} > 34.7GeV$:	(6.34±0.15)%	(92.23±1.02)%
$|E_{Cluster} - 38.0GeV| < 3.0GeV$:	(6.34±0.15)%	(92.27±1.03)%
$|E_{Cluster} - 38.0GeV| < 2.0GeV$:	(6.34±0.15)%	(92.61±1.06)%
$|E_{Cluster} - 18.8GeV| < 1.0GeV$:	(6.34±0.15)%	(93.23±1.21)%
$|E_{Cluster} - 18.8GeV| < 0.5GeV$:	(6.34±0.15)%	(93.80±1.58)%

identification efficiency at about 90% to find the corresponding pion fake rates. The results for 100GeV, 120GeV, 150GeV and 180GeV and their comparison with simple cut method are summarized in Table 19- 22 respectively. The neural network output plots with energies ratios only are shown in fig 30, and the neural network output plots with energies ratio and number of hit cells are shown in fig 31. If we assume the momentum is well measured, the neural network output plots with energies ratio and number of hit cells plus the information of E/P are shown in fig 32.

6 Conclusion

We study the separation of the electron and pion signals in the barrel electromagnetic calorimeter using the data from the test beam exposure of Module P15 to the electrons and pions in the momentum range from 20 to 180 GeV/c. Result using both simple cut and Neural Network methods are presented. We find that the spread of the shower through the layers of LARG described as the number of hit cells in these layers provide significant additional discriminative power. The study shows a good e$-\pi$ separation capability in the whole momentum range. Using information from the LARG only and allowing 90% electron identification efficiency, we

Table 13: The results for 40GeV using longitudinal and lateral profiles with Cherenkov tagging and various cuts on $E_{Cluster}$.

40 GeV Electron Samples Energy Ratios + Hit Cells	Electron Sample (Fake Rate)	Pion Sample (Efficiency)
By Cherenkov:	$(4.26\pm0.12)\%$	$(89.95\pm2.46)\%$
$E_{Cluster} > 34.7GeV$:	$(4.27\pm0.12)\%$	$(92.85\pm1.03)\%$
$|E_{Cluster} - 38.0GeV| < 3.0GeV$:	$(4.27\pm0.12)\%$	$(92.86\pm1.03)\%$
$|E_{Cluster} - 38.0GeV| < 2.0GeV$:	$(4.27\pm0.12)\%$	$(92.99\pm1.06)\%$
$|E_{Cluster} - 18.8GeV| < 1.0GeV$:	$(4.27\pm0.12)\%$	$(93.09\pm1.21)\%$
$|E_{Cluster} - 18.8GeV| < 0.5GeV$:	$(4.27\pm0.12)\%$	$(93.42\pm1.57)\%$

Table 14: The results for 40GeV using longitudinal and lateral profiles plus $E_{Cluster}/$P with Cherenkov tagging and various cuts on $E_{Cluster}$.

40 GeV Electron Samples Ratios+Hit Cells+$E_{Cluster}/40GeV > 0.8$	Electron Sample (Fake Rate)	Pion Sample (Efficiency)
By Cherenkov:	$(0.38\pm0.04)\%$	$(89.03\pm2.44)\%$
$E_{Cluster} > 34.7GeV$:	$(0.39\pm0.04)\%$	$(92.85\pm1.03)\%$
$|E_{Cluster} - 38.0GeV| < 3.0GeV$:	$(0.38\pm0.04)\%$	$(92.86\pm1.03)\%$
$|E_{Cluster} - 38.0GeV| < 2.0GeV$:	$(0.38\pm0.04)\%$	$(92.99\pm1.06)\%$
$|E_{Cluster} - 18.8GeV| < 1.0GeV$:	$(0.38\pm0.04)\%$	$(93.09\pm1.21)\%$
$|E_{Cluster} - 18.8GeV| < 0.5GeV$:	$(0.38\pm0.04)\%$	$(93.42\pm1.57)\%$

can achieve pion fake rate of $(1.8 - 3.2)\%$ with simple cuts. Assuming track momentum is well measured, the pion fake rates can be reduced to $(0.03 - 0.5)\%$ while maintaining 90% electron identification efficiency. Further significant improvements can be obtained by using Neural Network analysis method.

7   Acknowledgment

References

[1] ATLAS Collaboration, Technical Design Report, CERN/LHCC/96-41 (1996).

[2] M.Abouelouafa M.Gouanere and P.Perrodo,Trigger setup in H8 and H6 Test Beam Area

Table 15: The results for 100GeV using simple cuts on longitudinal profile, lateral profile, longitudinal and lateral profiles plus $E_{Cluster}/P$.

100 GeV Sample by $E_{Cluster}$ Cut: $E_{Cluster} > 89.5$GeV	Electron Sample (Efficiency)	Pion Sample (Fake Rate)
After Quality and $E_{Cluster}$ Cut:	11162	16337
$E_{Cluster} > 0$, $0.005 < E_0/E_{Cluster} < 0.07$, $E_{11}/E_{Cluster} > 0.55$ $E_3/E_{Cluster} < 0.014$, $E_2/E_{Cluster} > 0.65$ $0.05 < E_1/E_{Cluster} < 0.3$	10045 (89.99±1.24)%	218 (1.33±0.09)%
$E_{Cluster} > 0$, $0.005 < E_0/E_{Cluster} < 0.07$, $E_{11}/E_{Cluster} > 0.55$ $E_3/E_{Cluster} < 0.015$, $E_2/E_{Cluster} > 0.6$ $0.05 < E_1/E_{Cluster} < 0.35$ $NH(0) > 0, NH(1) > 8, NH(2) > 7, NH(3) > 0$	10172 (91.13±1.25)%	169 (1.03±0.08)%
Above Energy Ratio and Number of Hit Cell cuts $E_{Cluster}/100.0$GeV > 0.90	10123 (90.69±1.24)%	5 (0.03±0.01)%

[3] EMTB User Guide Version 1-10, Remi Lafaye, Delphine Nicod, Dirk Zerwas, Robert Zitoun

[4] W.E. Cleland and E.G. Stern, Nucl. Instrum. Methods A 338 (1994) 467.

[5] R.Mehdiyev et al. ATLAS Calorimetry Note ATL-CAL-99-002, 1999.

[6] CERN-EP/2002-087 Preprint (November 7, 2002)

[7] Cranmer, K.; Mcnamara, P.; Mellado, B.; Pan, Y.; Quayle, W.; Wu, Sau Lan; ATL-PHYS-2003-007

[8] J.Schwindling B.Mansoulie, Using Multi-Layer Perceptrons in PAW

Table 16: The results for 120GeV using simple cuts on longitudinal profile, lateral profile, longitudinal and lateral profiles plus $E_{Cluster}/P$.

120 GeV Sample by $E_{Cluster}$ Cut: $E_{Cluster} > 108.5$GeV	Electron Sample (Efficiency)	Pion Sample (Fake Rate)
After Quality and $E_{Cluster}$ Cut:	9474	85704
$E_{Cluster} > 0$, $0.005 < E_0/E_{Cluster} < 0.055$, $E_{11}/E_{Cluster} > 0.55$ $E_3/E_{Cluster} < 0.015$, $E_2/E_{Cluster} > 0.65$	8560 (90.35±1.35)%	933 (1.09±0.04)%
$E_{Cluster} > 0$, $0.005 < E_0/E_{Cluster} < 0.06$, $E_{11}/E_{Cluster} > 0.55$ $0.005 < E_3/E_{Cluster} < 0.015$, $E_2/E_{Cluster} > 0.6$ $NH(0) > 0, NH(1) > 9, NH(2) > 7, NH(3) > 0$	8626 (91.05±1.36)%	704 (0.82±0.03)%
Above Energy Ratio and Number of Hit Cell cuts $E_{Cluster}/120.0$GeV > 0.90	8626 (91.05±1.36)%	22 (0.03±0.01)%

Table 17: The results for 150GeV using simple cuts on longitudinal profile, lateral profile, longitudinal and lateral profiles plus $E_{Cluster}/P$.

150 GeV Sample by $E_{Cluster}$ Cut: $E_{Cluster} > 136.5$GeV	Electron Sample (Efficiency)	Pion Sample (Fake Rate)
After Quality and $E_{Cluster}$ Cut:	4072	37495
$E_{Cluster} > 0$, $0.005 < E_0/E_{Cluster} < 0.055$, $E_{11}/E_{Cluster} > 0.55$ $0.006 < E_3/E_{Cluster} < 0.015$, $E_2/E_{Cluster} > 0.65$ $0.05 < E_1/E_{Cluster} < 0.3$	3666 (90.03±2.05)%	468 (1.25±0.06)%
$E_{Cluster} > 0$, $0.005 < E_0/E_{Cluster} < 0.055$, $E_{11}/E_{Cluster} > 0.55$ $0.006 < E_3/E_{Cluster} < 0.015$, $E_2/E_{Cluster} > 0.65$ $0.05 < E_1/E_{Cluster} < 0.3$ $NH(0) > 0, NH(1) > 10, NH(2) > 7, NH(3) > 1$	3632 (89.19±2.04)%	346 (0.92±0.05)%
Above Energy Ratio and Number of Hit Cell cuts $E_{Cluster}/150.0$GeV > 0.90	3632 (89.19±2.04)%	11 (0.03±0.01)%

Table 18: The results for 180GeV using simple cuts on longitudinal profile, lateral profile, longitudinal and lateral profiles plus $E_{Cluster}$/P.

180 GeV Sample by $E_{Cluster}$ Cut: $E_{Cluster} > 170.5$GeV	Electron Sample (Efficiency)	Pion Sample (Fake Rate)
After Quality and $E_{Cluster}$ Cut:	8344	75338
$E_{Cluster} > 0$, $0.005 < E_0/E_{Cluster} < 0.045$, $E_{11}/E_{Cluster} > 0.45$ $0.006 < E_3/E_{Cluster} < 0.016$, $E_2/E_{Cluster} > 0.7$ $0.05 < E_1/E_{Cluster} < 0.3$	7492 $(89.79\pm1.43)\%$	1540 $(2.04\pm0.05)\%$
$E_{Cluster} > 0$, $0.005 < E_0/E_{Cluster} < 0.05$, $E_{11}/E_{Cluster} > 0.4$ $E_3/E_{Cluster} < 0.015$, $E_2/E_{Cluster} > 0.65$ $NH(0) > 0$, $NH(1) > 11$, $NH(2) > 7$, $NH(3) > 1$	7568 $(90.70\pm1.44)\%$	1362 $(1.81\pm0.05)\%$
Above Energy Ratio and Number of Hit Cell cuts $E_{Cluster}/180.0$GeV > 0.90	7568 $(90.70\pm1.44)\%$	30 $(0.04\pm0.01)\%$

Table 19: The results for 100GeV using Neural Network method and the comparison with simple cut method.

100 GeV with 90% Electron Efficiency	Fake Rate (CUT)	Fake Rate (NN)
Energy Ratio	$(1.33\pm0.09)\%$	$(1.08\pm0.13)\%$
Energy Ratio + Hit Cells	$(1.03\pm0.08)\%$	$(0.48\pm0.09)\%$
Ratio+Hit Cells+$E_{Cluster}/100GeV$	$(0.03\pm0.01)\%$	$(0.06\pm0.03)\%$

Table 20: The results for 120GeV using Neural Network method and the comparison with simple cut method.

120 GeV with 90% Electron Efficiency	Fake Rate (CUT)	Fake Rate (NN)
Energy Ratio	$(1.09\pm0.04)\%$	$(0.50\pm0.04)\%$
Energy Ratio + Hit Cells	$(0.82\pm0.03)\%$	$(0.19\pm0.02)\%$
Ratio+Hit Cells+$E_{Cluster}/120GeV$	$(0.03\pm0.01)\%$	$(0.01\pm0.01)\%$

Table 21: The results for 150GeV using Neural Network method and the comparison with simple cut method.

150 GeV with 90% Electron Efficiency	Fake Rate (CUT)	Fake Rate (NN)
Energy Ratio	$(1.25\pm0.06)\%$	$(1.15\pm0.08)\%$
Energy Ratio + Hit Cells	$(0.92\pm0.05)\%$	$(0.49\pm0.05)\%$
Ratio+Hit Cells+$E_{Cluster}/150GeV$	$(0.03\pm0.01)\%$	$(0.07\pm0.02)\%$

Table 22: The results for 180GeV using Neural Network method and the comparison with simple cut method.

180 GeV with 90% Electron Efficiency	Fake Rate (CUT)	Fake Rate (NN)
Energy Ratio	$(2.04\pm0.05)\%$	$(0.52\pm0.03)\%$
Energy Ratio + Hit Cells	$(1.81\pm0.05)\%$	$(0.50\pm0.03)\%$
Ratio+Hit Cells+$E_{Cluster}/180GeV$	$(0.04\pm0.01)\%$	$(0.04\pm0.02)\%$
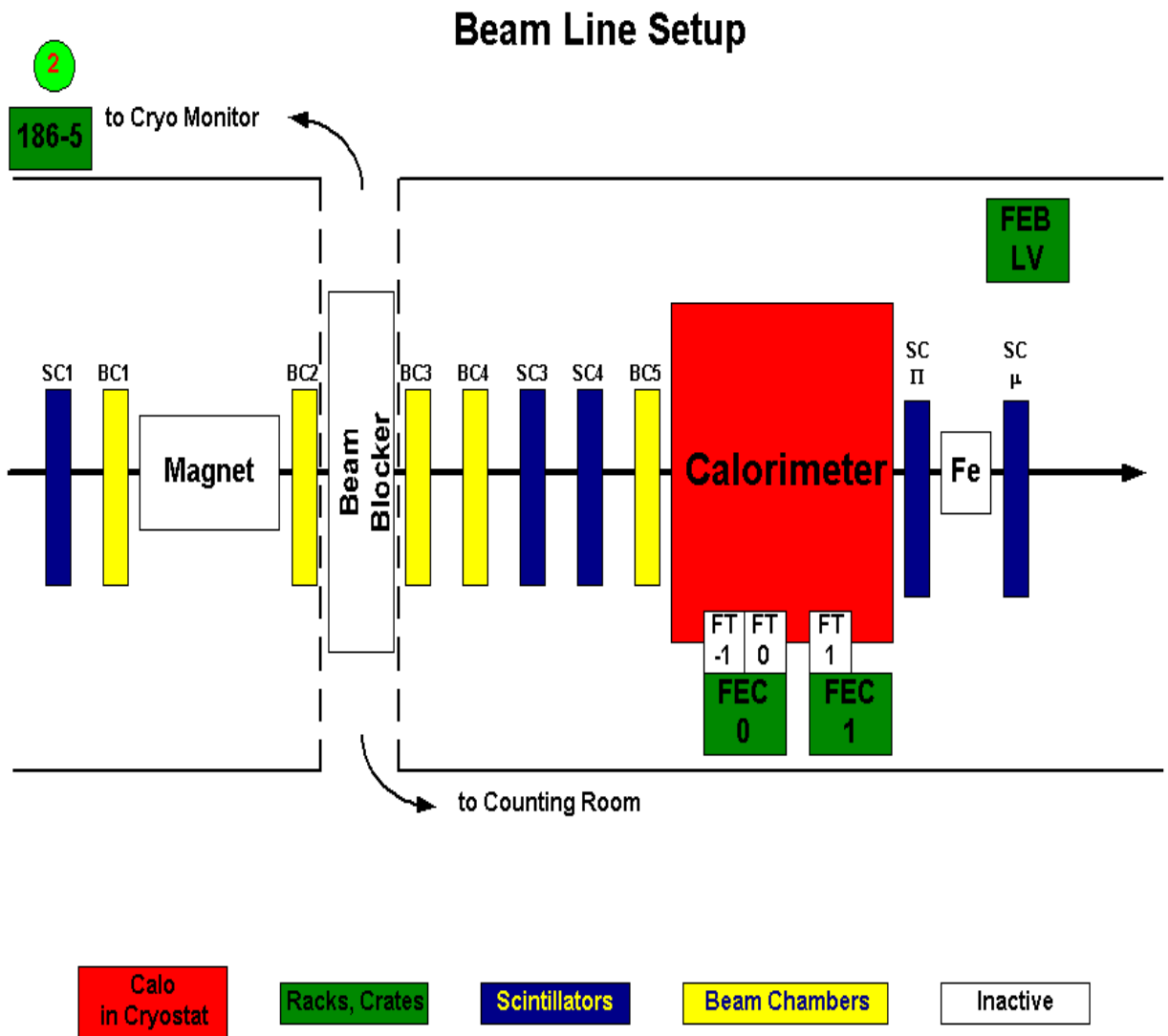
Figure 1: The Testbeam setup during June/July 2002 EM barrel module P15 testbeam data taking. The scintillator SC1,SC3 and SC4 are used to define the beam and reject pions. Beam chambers BC1 though BC4 give the X and Y positions when the particle passing by those beam chambers. Scintillator SCπ and SCμ provide the ADC counts to reject pions and muons separately.
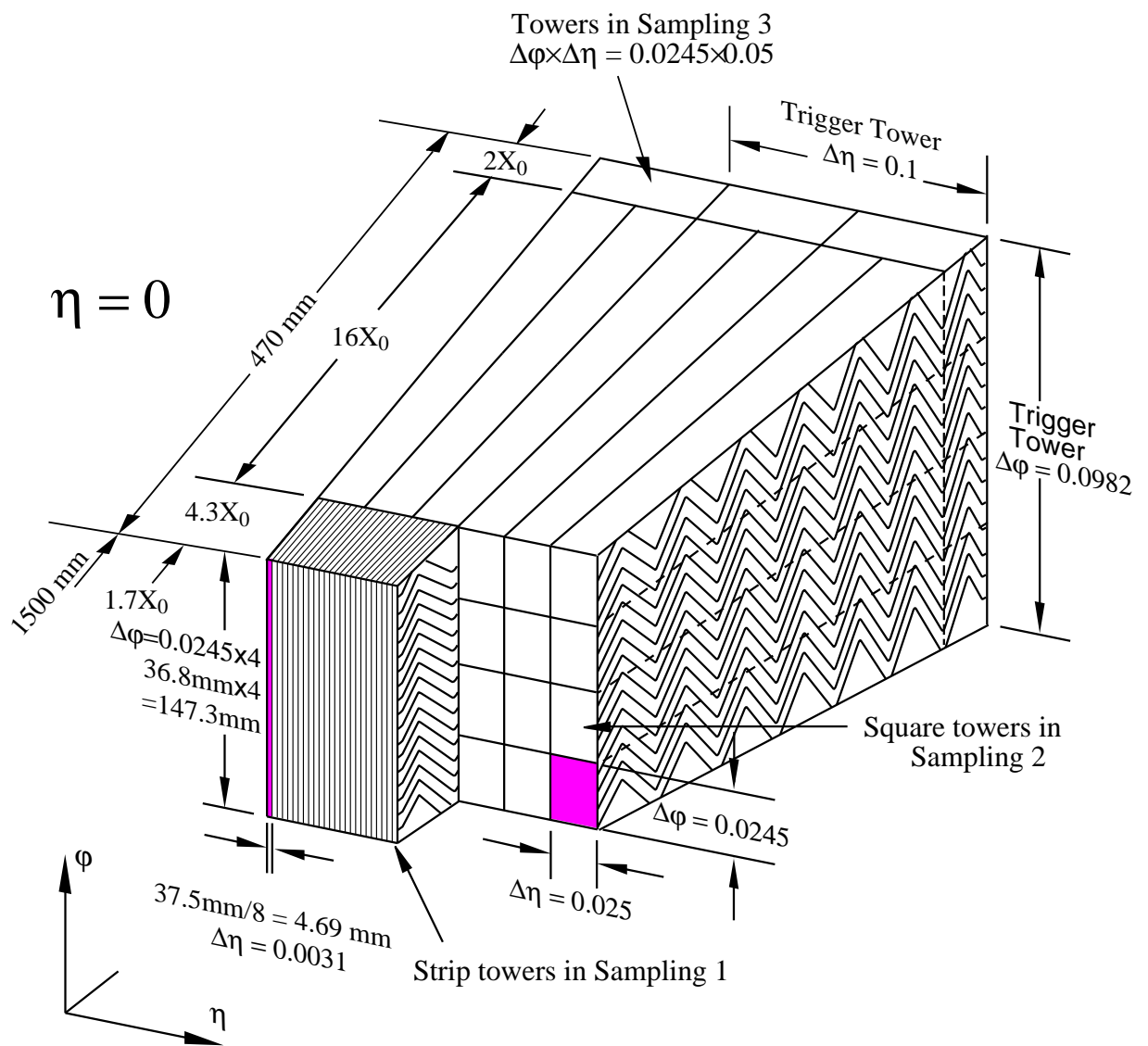
Figure 2: The readout cells definitions.
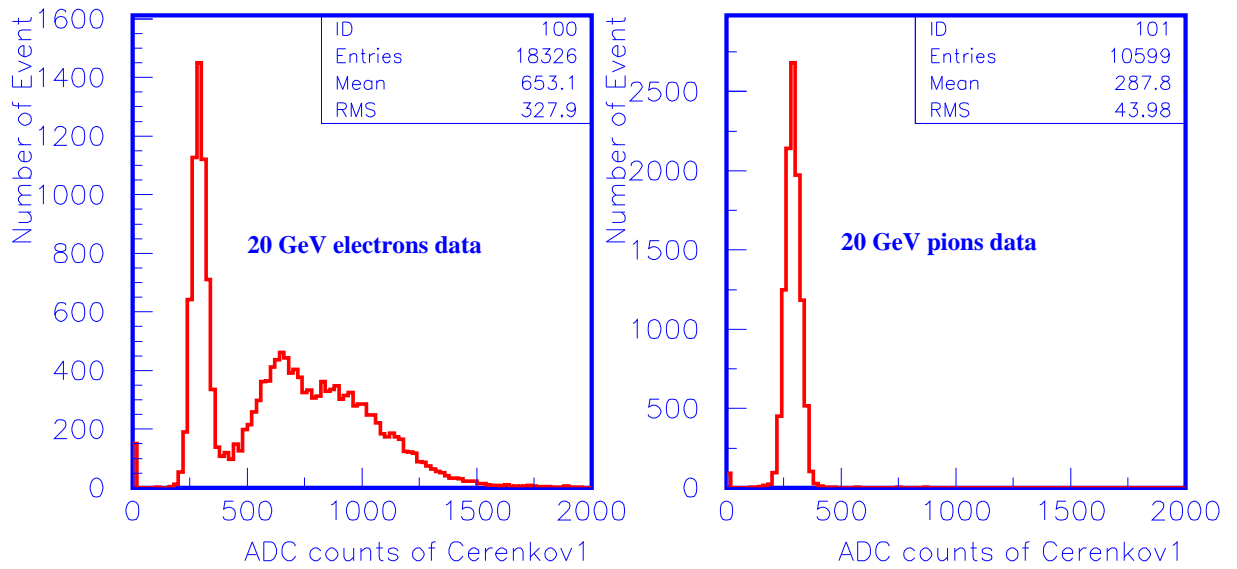
Figure 3: The Cherenkov signal for 20 GeV electron run and pion run.

20 GeV

Presampler

ID	201
Entries	10275
Mean	0.1860
RMS	0.3364

Layer 1

ID	301
Entries	10275
Mean	0.5450
RMS	0.9095

Layer 2

ID	401
Entries	10275
Mean	3.739
RMS	3.424

Layer 3

ID	500
Entries	18882
Mean	0.1240
RMS	0.8117E-01

Total Energy

ID	600
Entries	18882
Mean	18.59
RMS	0.7006

Enger, GeV/c^2

40 GeV

Presampler

ID	201
Entries	30312
Mean	0.2953
RMS	0.5140

Layer 1

ID	301
Entries	30312
Mean	1.112
RMS	1.653

Layer 2

ID	401
Entries	30312
Mean	8.103
RMS	7.003

Layer 3

ID	500
Entries	17032
Mean	0.2875
RMS	0.1322

Total Energy

ID	600
Entries	17032
Mean	37.63
RMS	0.9404

Enger, GeV/c^2

Figure 4: The energy deposited in each layer of the calorimeter and the total energy deposition for the 20 and 40 GeV/c electron and pion beams. All plots are normalized to 1 and the solid line stand for electrons and dash line stand for pions.

20
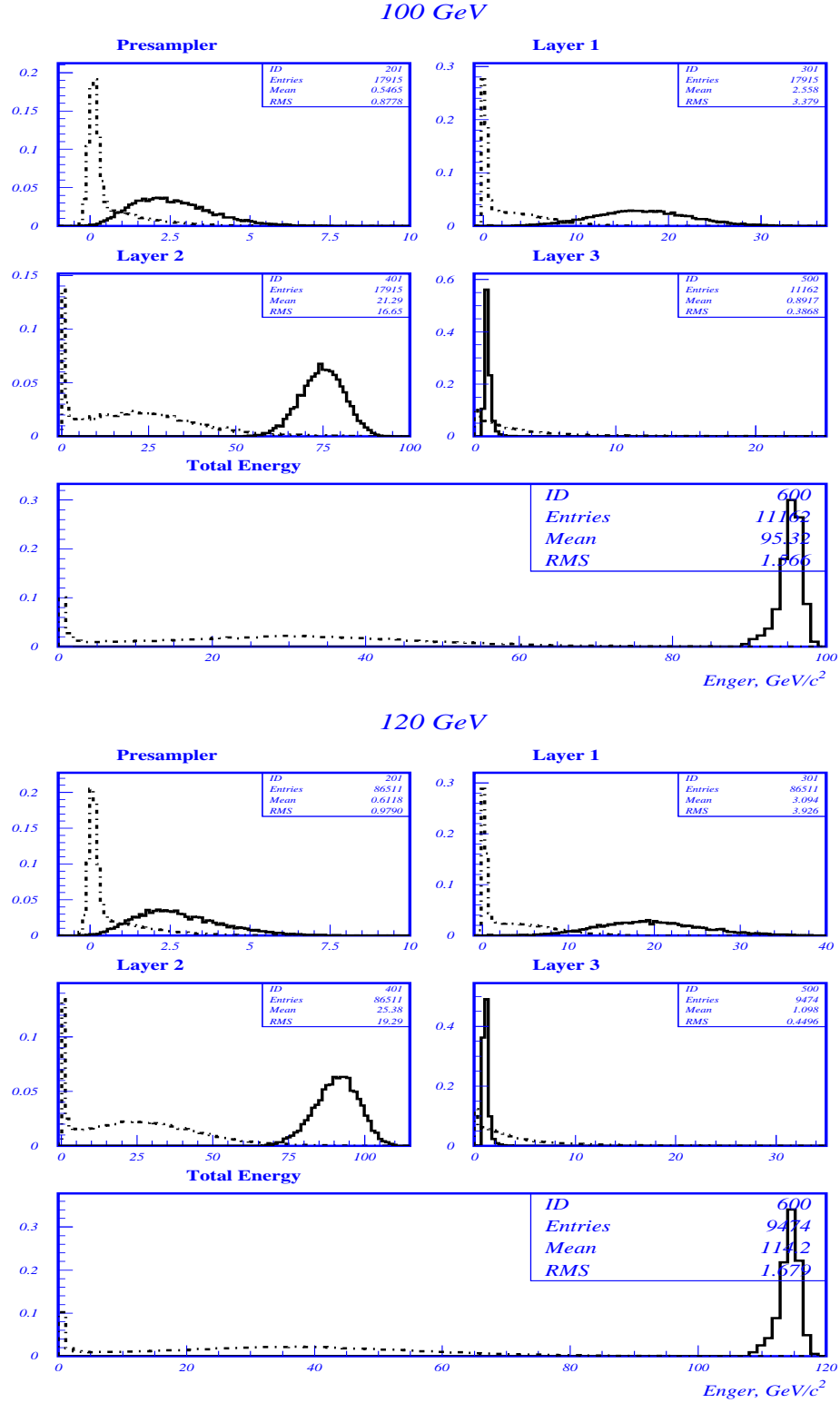
Figure 5: The energy deposited in each layer of the calorimeter and the total energy deposition for the 100 and 120 GeV/c electron and pion beams. All plots are normalized to 1 and the solid line stand for electrons and dash line stand for pions.

21

150 GeV

Presampler

ID	201
Entries	43192
Mean	0.7174
RMS	1.147

Layer 1

ID	301
Entries	43192
Mean	3.766
RMS	4.763

Layer 2

ID	401
Entries	43192
Mean	32.56
RMS	24.70

Layer 3

ID	500
Entries	4072
Mean	1.460
RMS	0.6611

Total Energy

ID	600
Entries	4072
Mean	143.8
RMS	1.995

Enger, GeV/c^2

180 GeV

Presampler

ID	201
Entries	94195
Mean	0.8129
RMS	1.291

Layer 1

ID	301
Entries	94195
Mean	4.523
RMS	5.711

Layer 2

ID	401
Entries	94195
Mean	40.37
RMS	30.65

Layer 3

ID	500
Entries	8344
Mean	1.796
RMS	0.7885

Total Energy

ID	600
Entries	8344
Mean	172.9
RMS	1.454

Enger, GeV/c^2

Figure 6: The energy deposited in each layer of the calorimeter and the total energy deposition for the 150 and 180 GeV/c electron and pion beams. All plots are normalized to 1 and the solid line stand for electrons and dash line stand for pions.

22
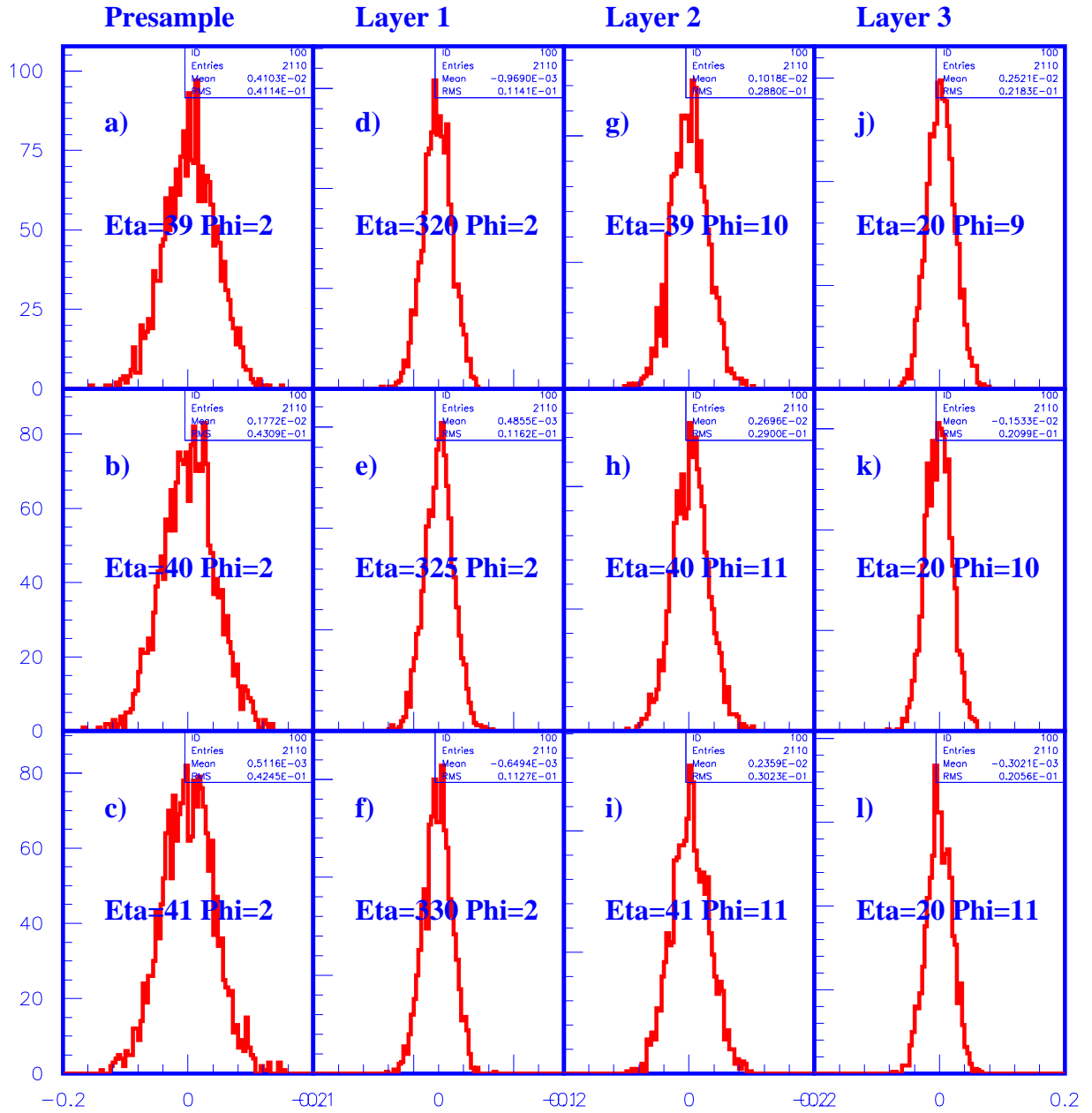
Figure 7: The noise level (pedestals) for selected cells of the calorimeter using random trigger. In general, the pedestals in all the cells in the same layer are similar.
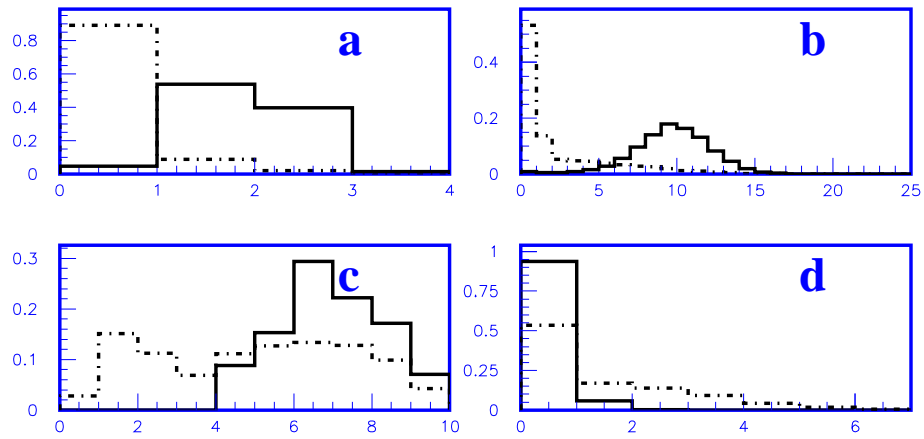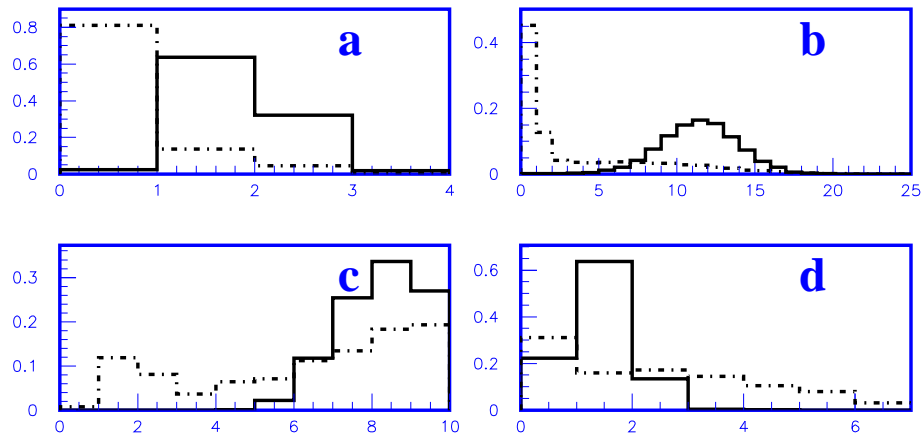
Figure 8: The number of hit cells for 20 and 40 GeV electrons and pions for a) presampler, b) front layer, c)middle layer and d) back layers of the calorimeter. All plots are normalized to 1 and solid line stand for electrons and dash line stand for pions.
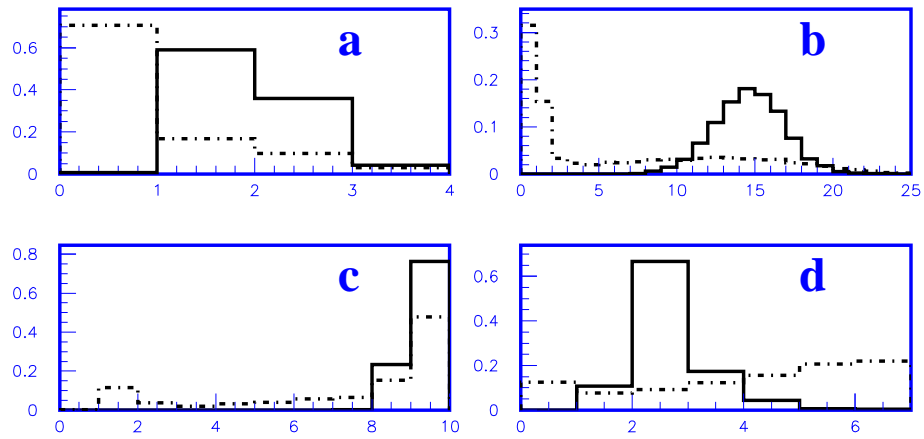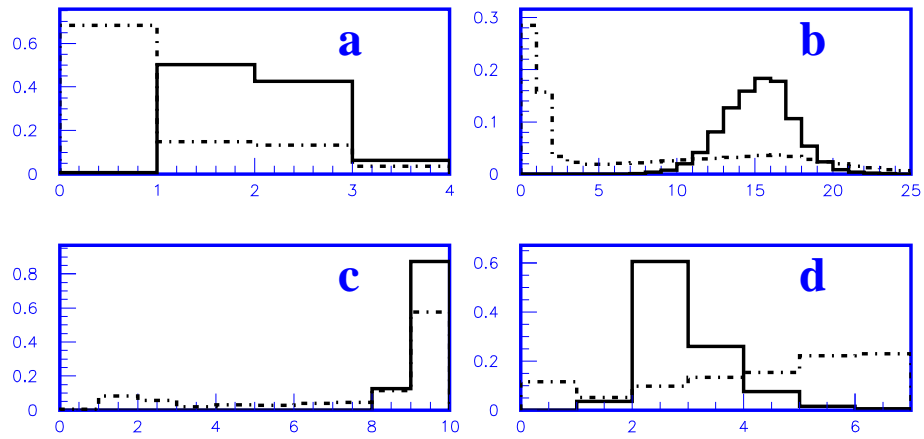
Figure 9: The number of hits for 100 and 120 GeV electrons and pions for a) presampler, b) front layer, c)middle layer and d) back layers of the calorimeter. All plots are normalized to 1 and solid line stand for electrons and dash line stand for pions.
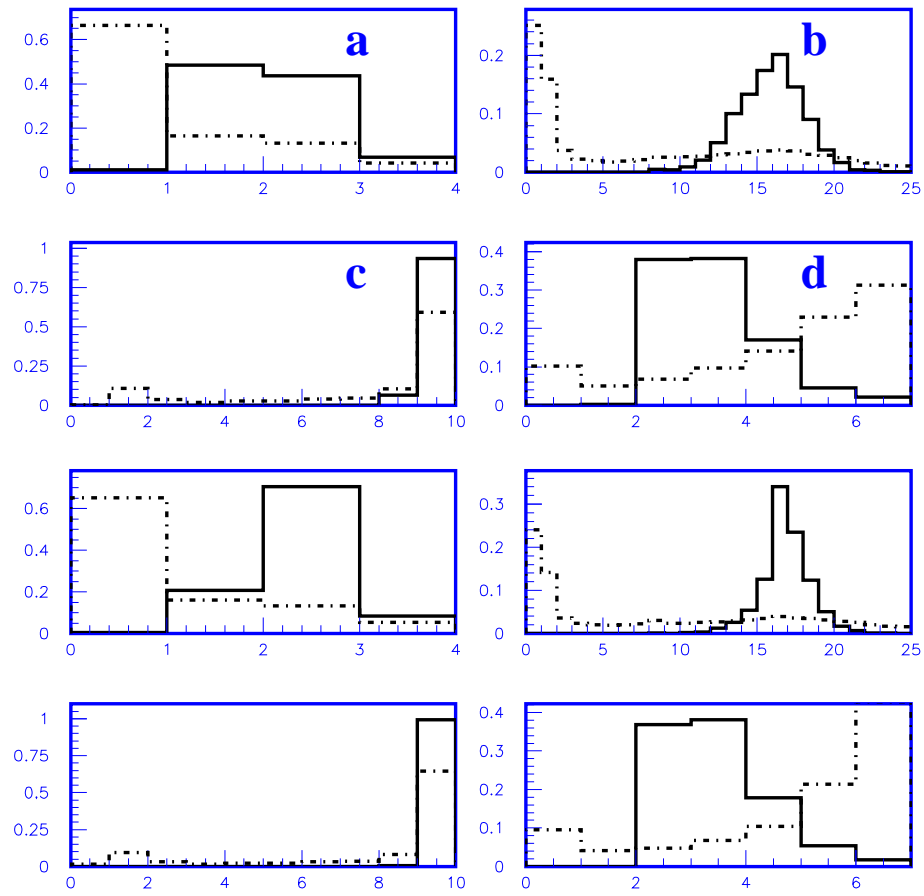
Figure 10: The number of hits for 150 and 180 GeV electrons and pions for a) presampler, b) front layer, c)middle layer and d) back layers of the calorimeter. All plots are normalized to 1 and solid line stand for electrons and dash line stand for pions.
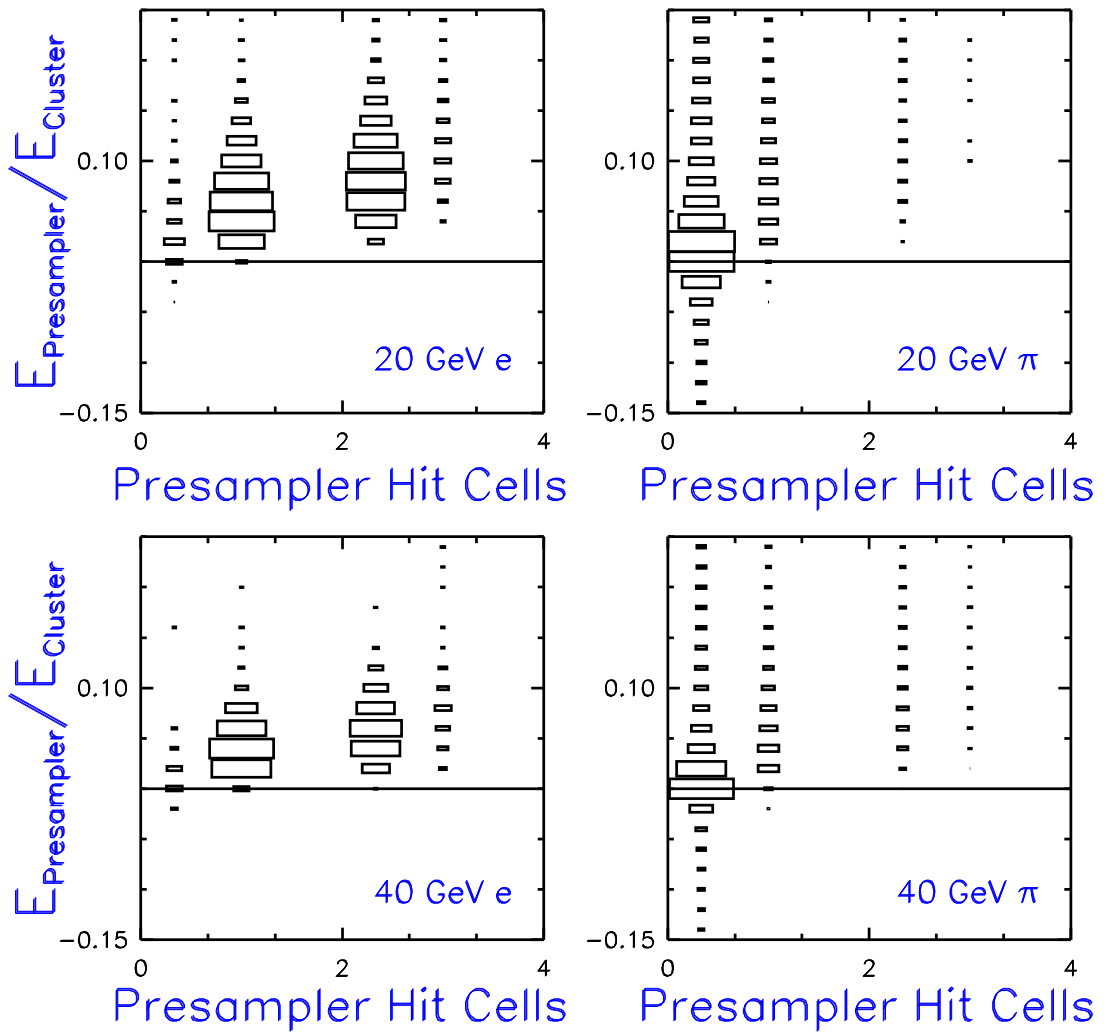
Figure 11: Number of Presampler hit cells vs $E_{Presampler}/E_{Cluster}$ 2d plots for 20GeV and 40GeV e and π samples
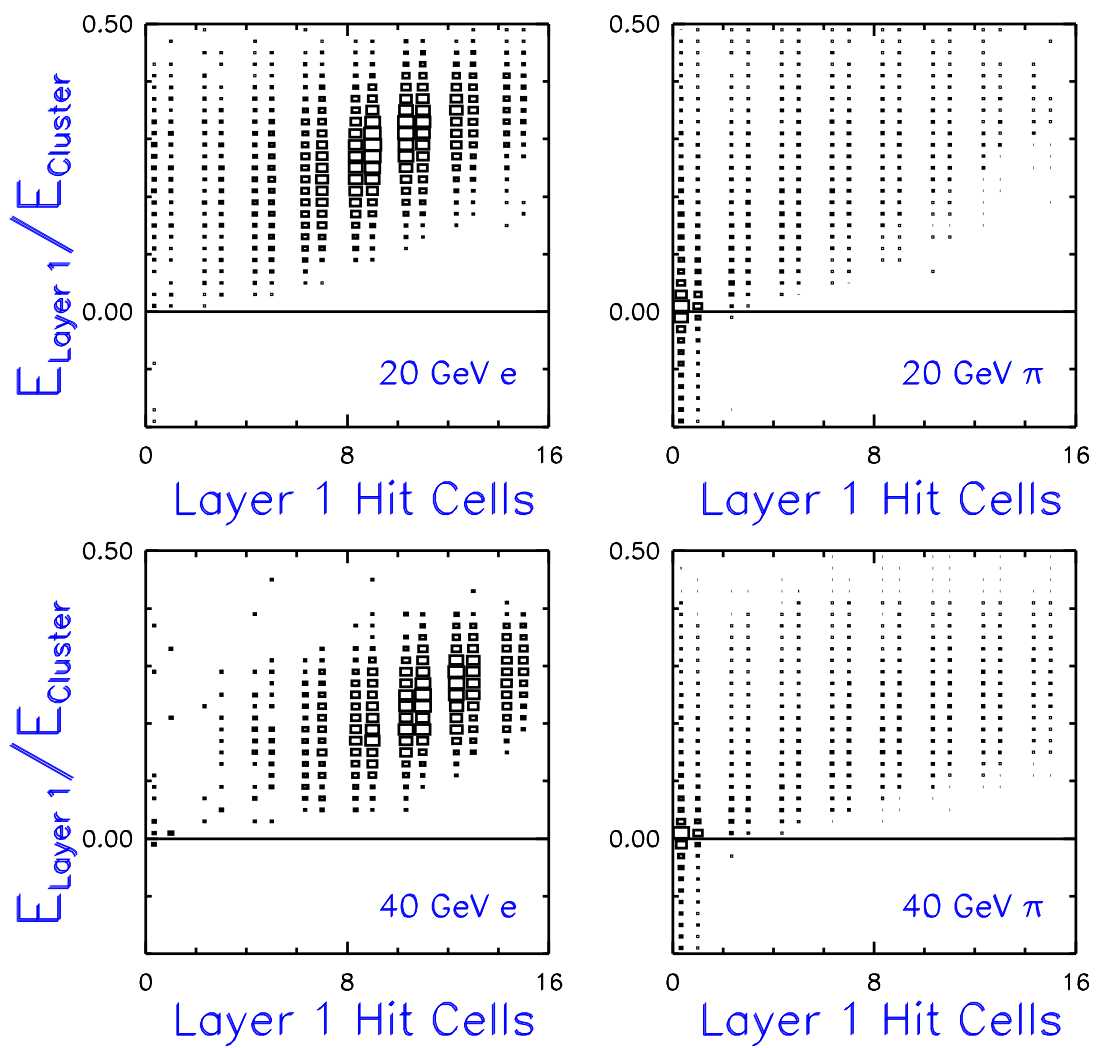
Figure 12: Number of Layer 1 hit cells vs $E_{Layer1}/E_{Cluster}$ 2d plots for 20GeV and 40GeV e and π samples.
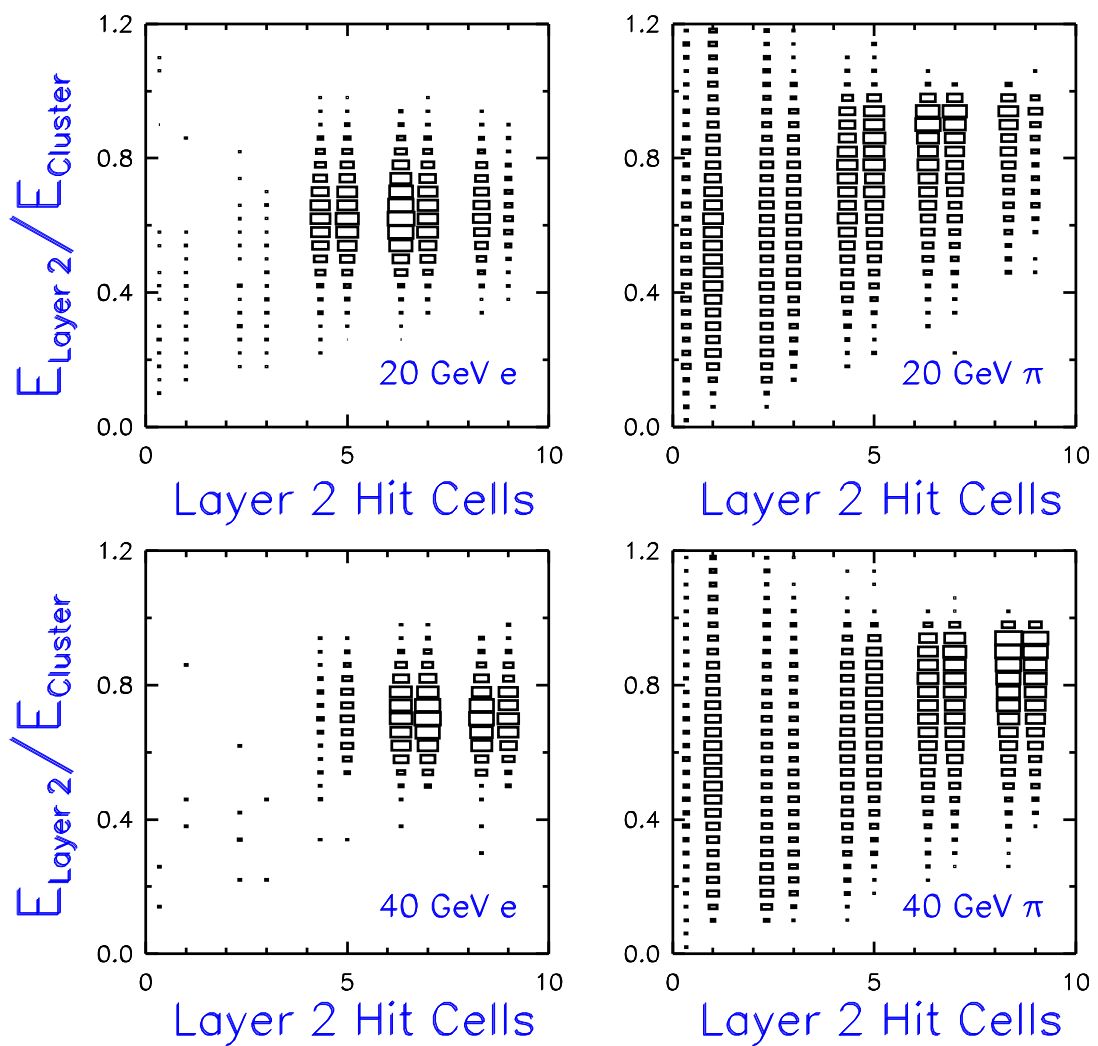
Figure 13: Number of Layer 2 hit cells vs $E_{Layer2}/E_{Cluster}$ 2d plots for 20GeV and 40GeV e and π samples.
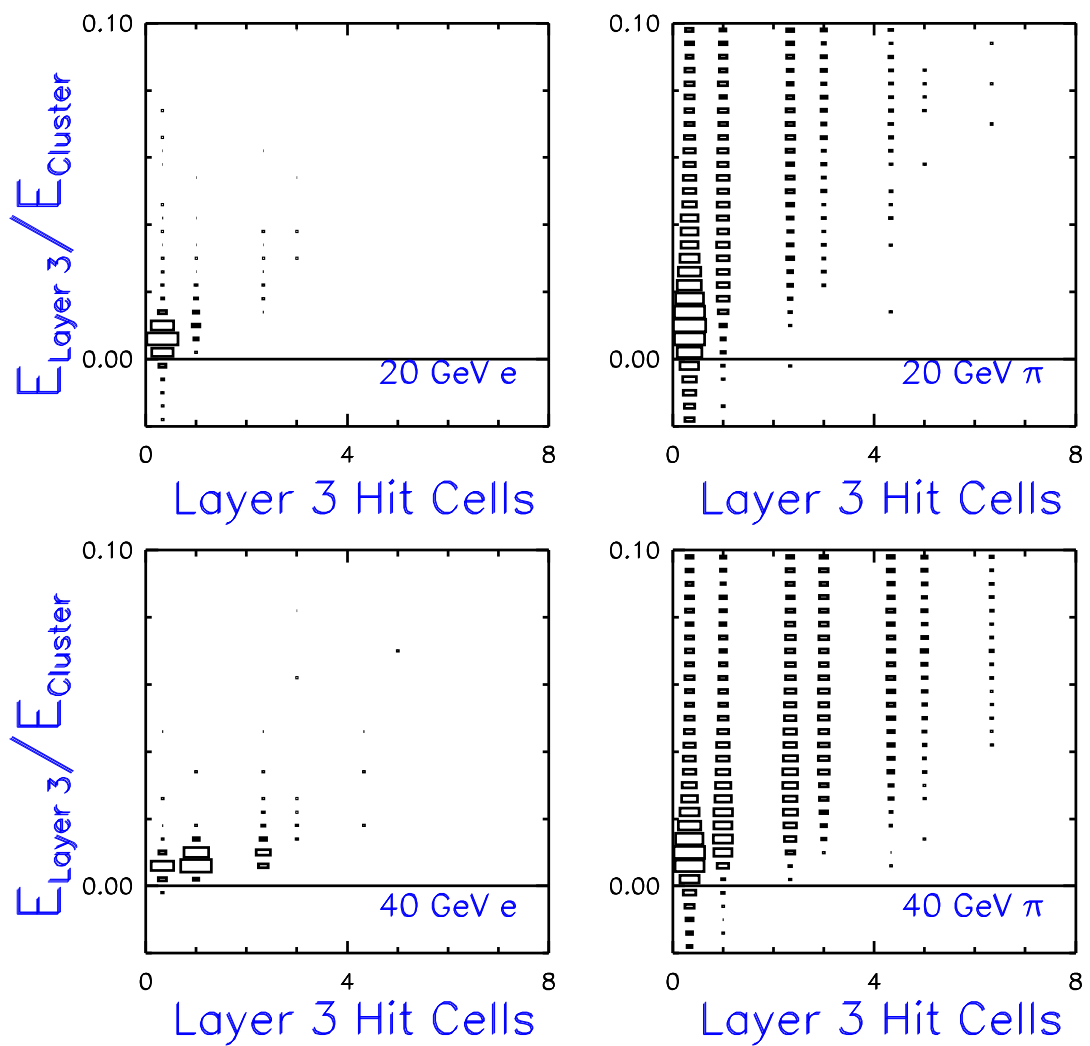
Figure 14: Number of Layer 3 hit cells vs $\mathrm{E}_{Layer3}/\mathrm{E}_{Cluster}$ 2d plots for 20GeV and 40GeV e and π samples/
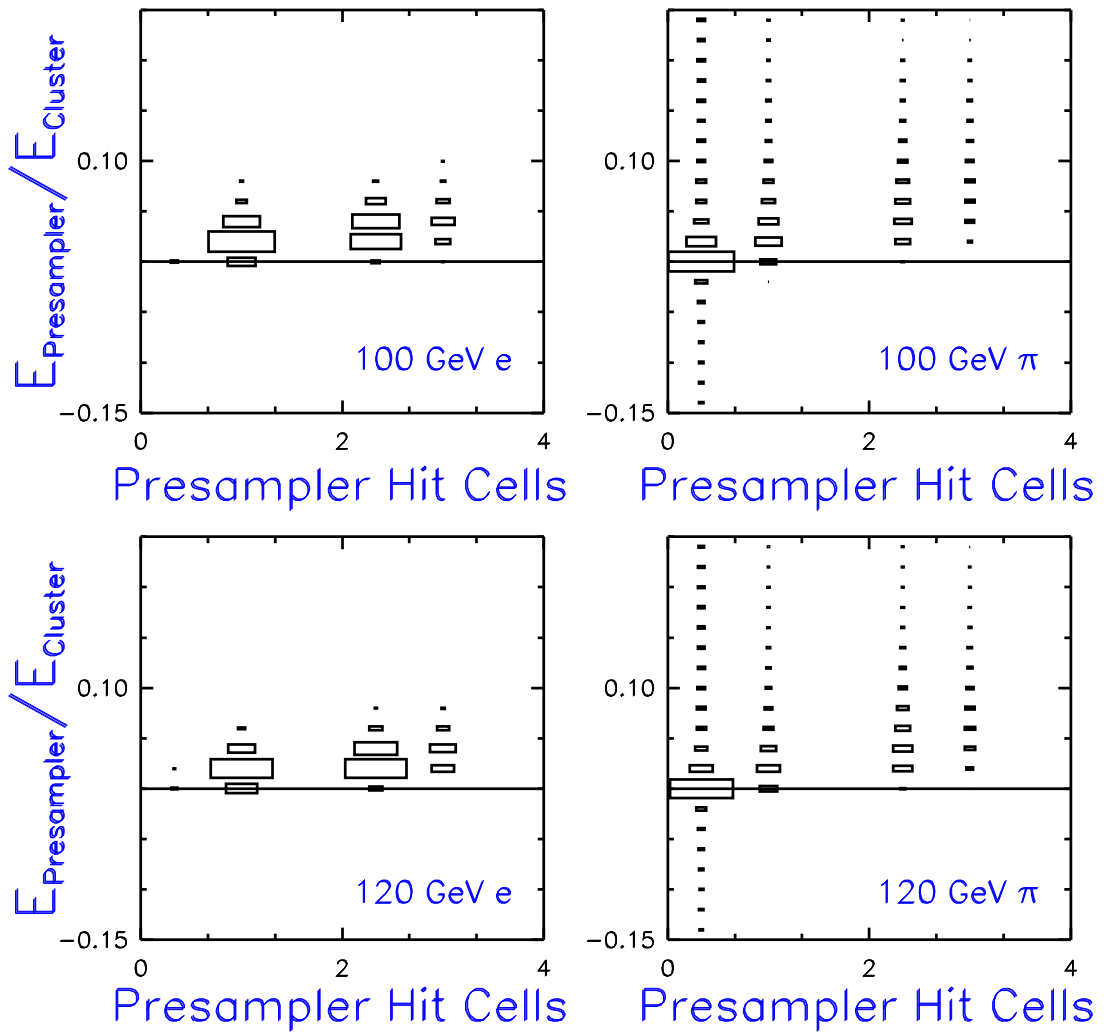
Figure 15: Number of Presampler hit cells vs $\mathrm{E}_{Presampler}/\mathrm{E}_{Cluster}$ 2d plots for 100GeV and 120GeV e and π samples.
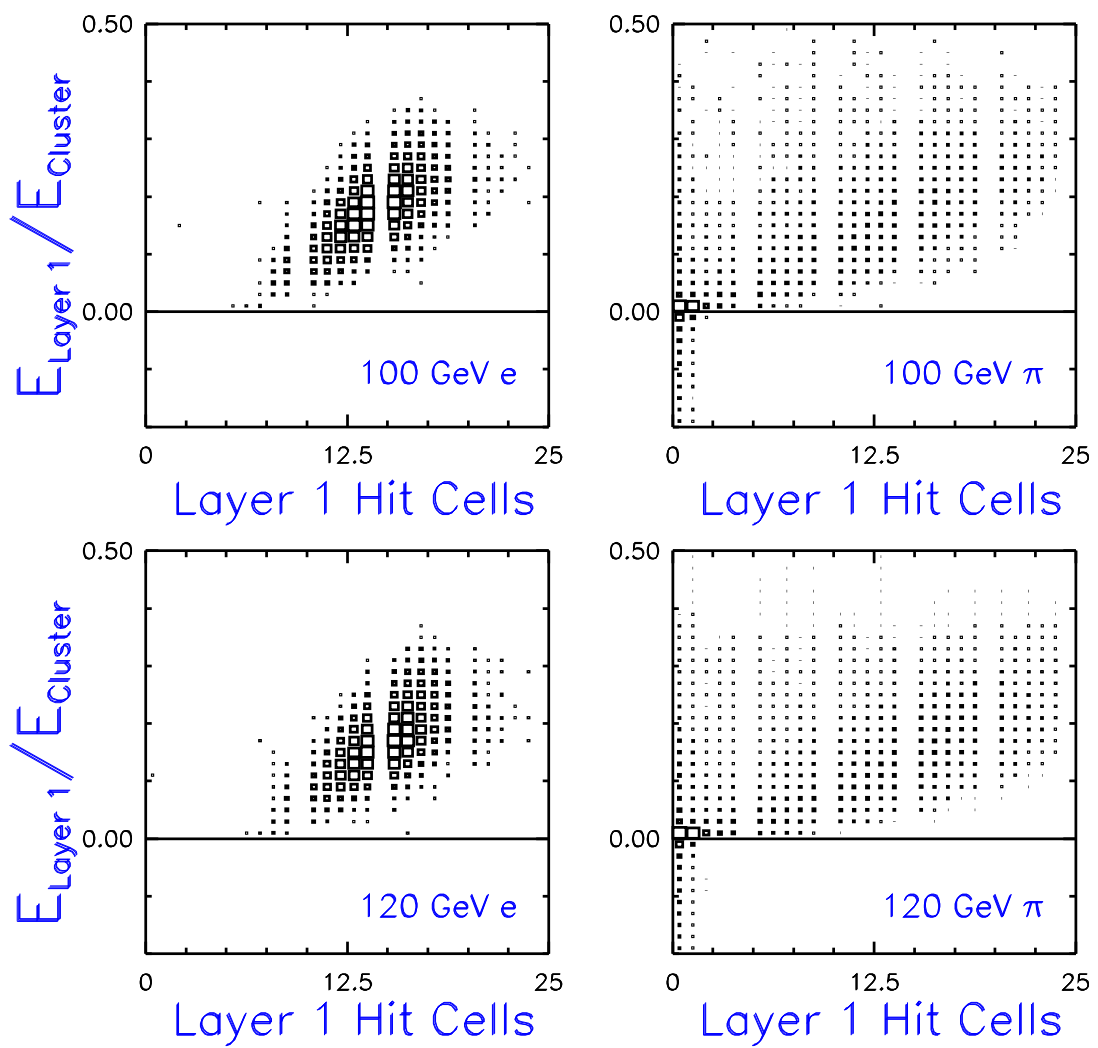
Figure 16: Number of Layer 1 hit cells vs $E_{Layer1}/E_{Cluster}$ 2d plots for 100GeV and 120GeV e and π samples.
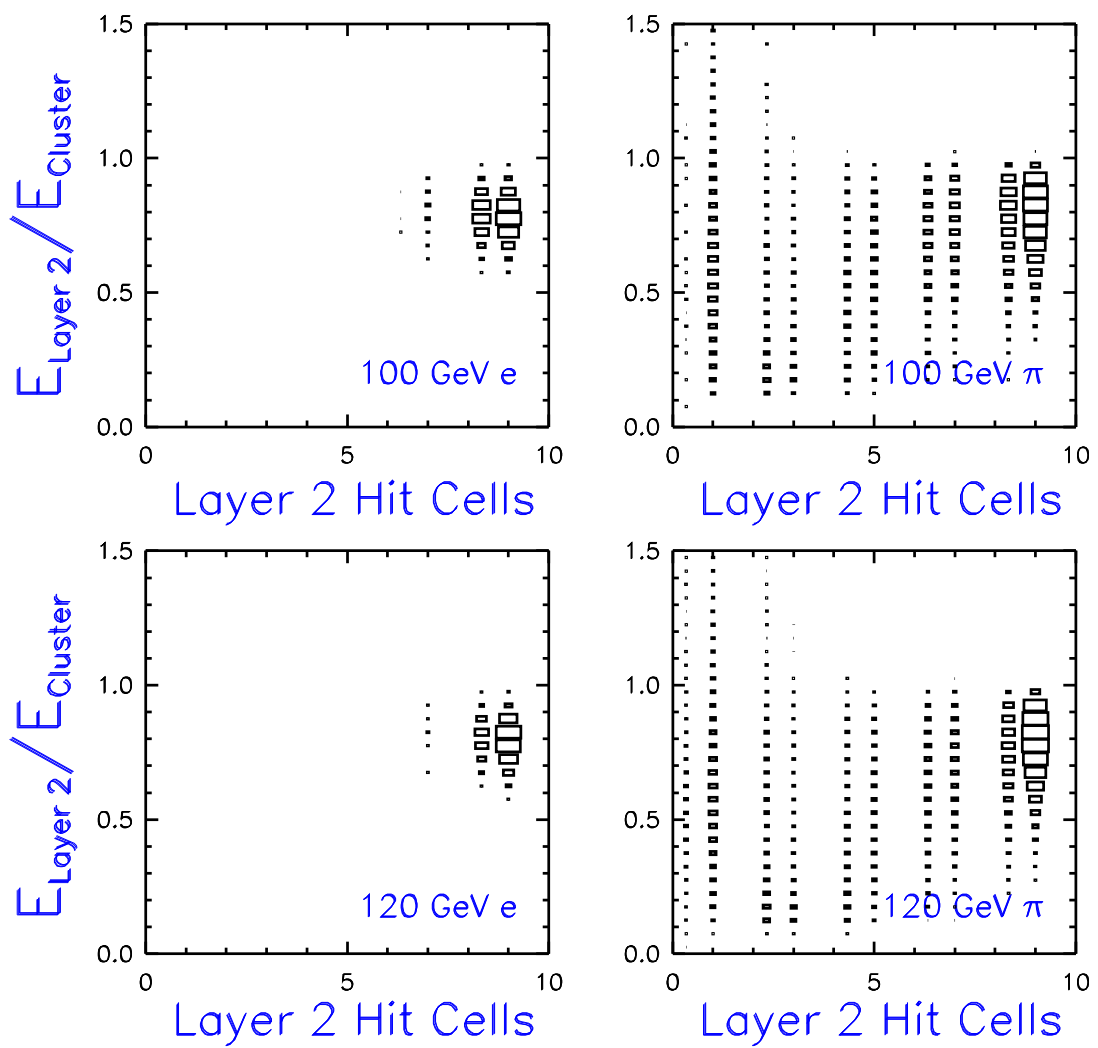
Figure 17: Number of Layer 2 hit cells vs $\mathrm{E}_{Layer2}/\mathrm{E}_{Cluster}$ 2d plots for 100GeV and 120GeV e and π samples.
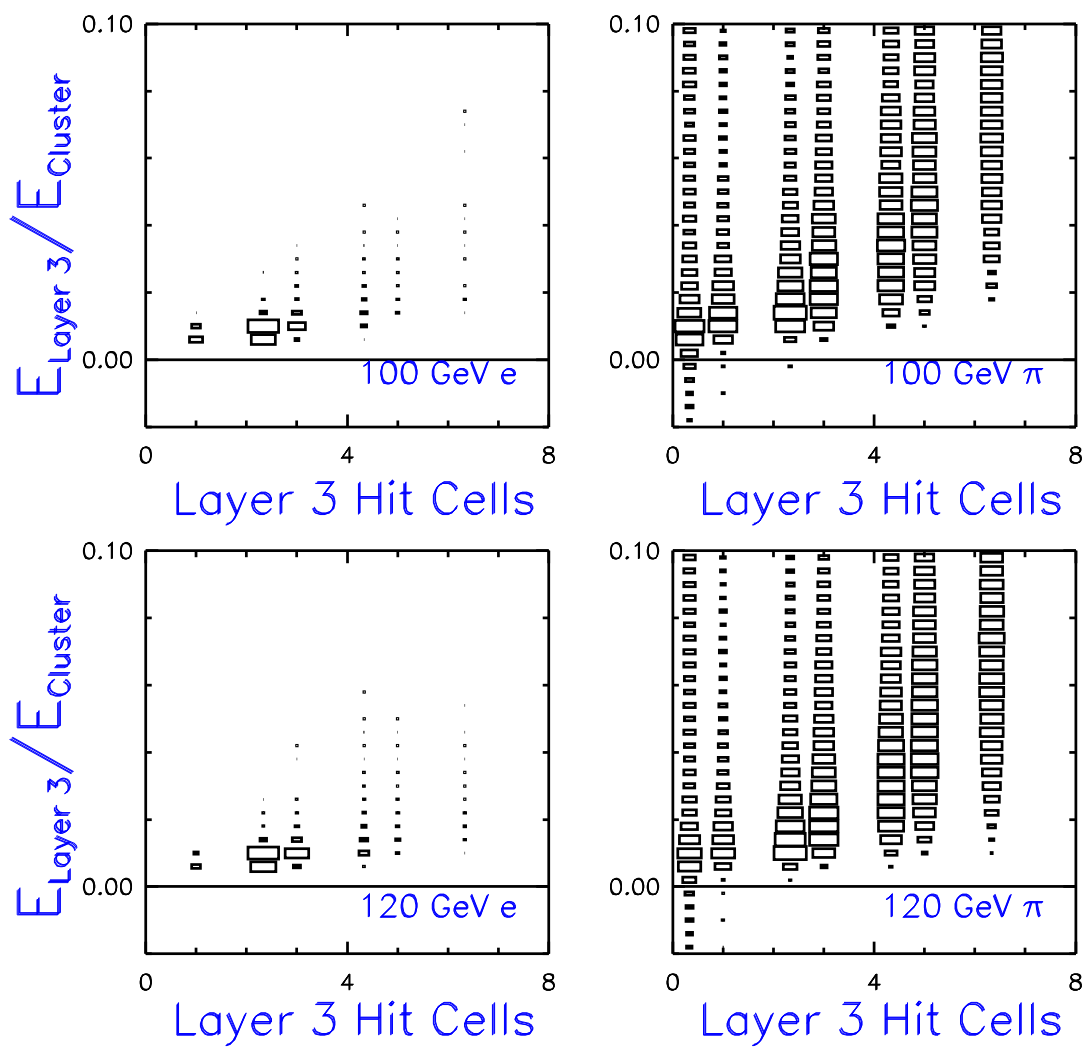
Figure 18: Number of Layer 3 hit cells vs $E_{Layer3}/E_{Cluster}$ 2d plots for 100GeV and 120GeV e and π samples.
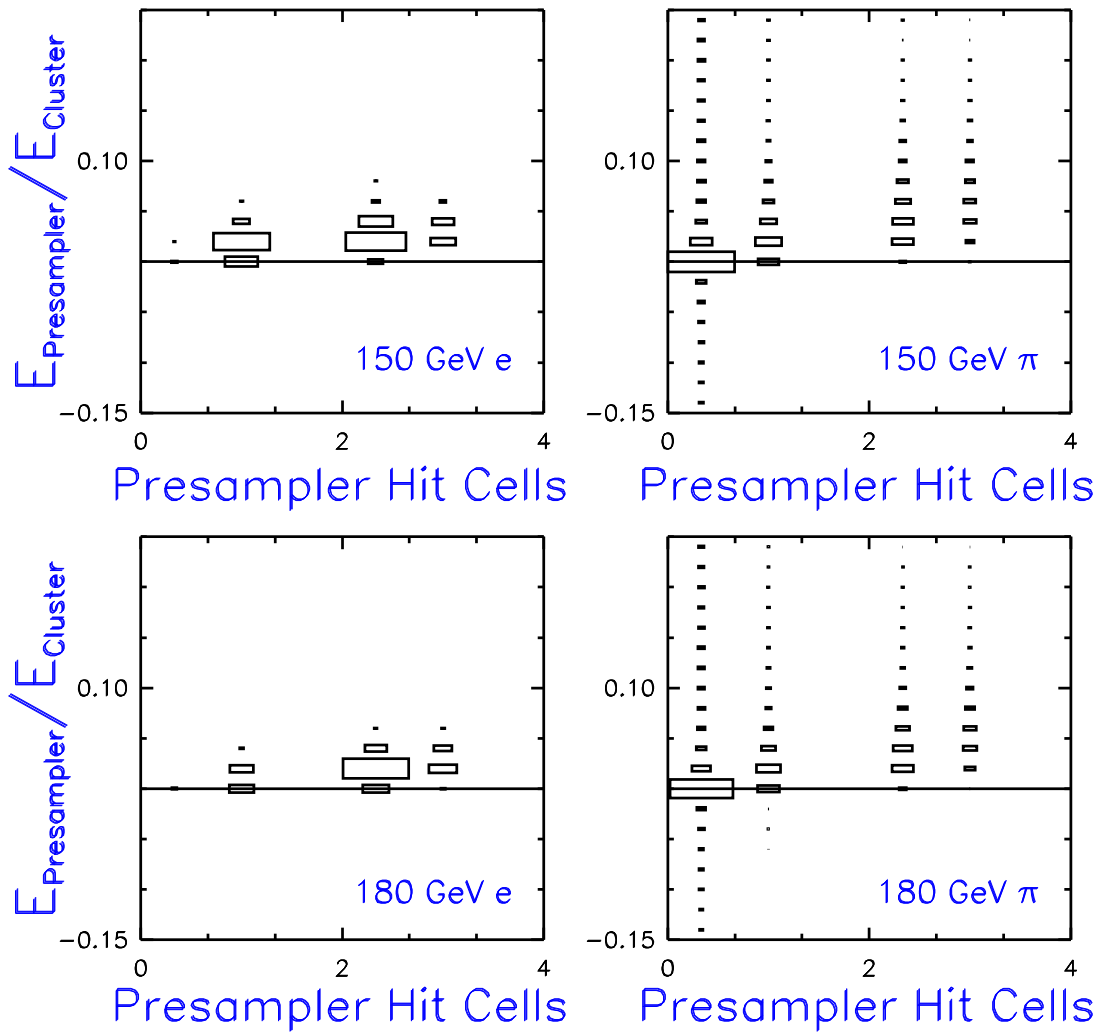
Figure 19: Number of Presampler hit cells vs $E_{Presampler}/E_{Cluster}$ 2d plots for 150GeV and 180GeV e and π samples.
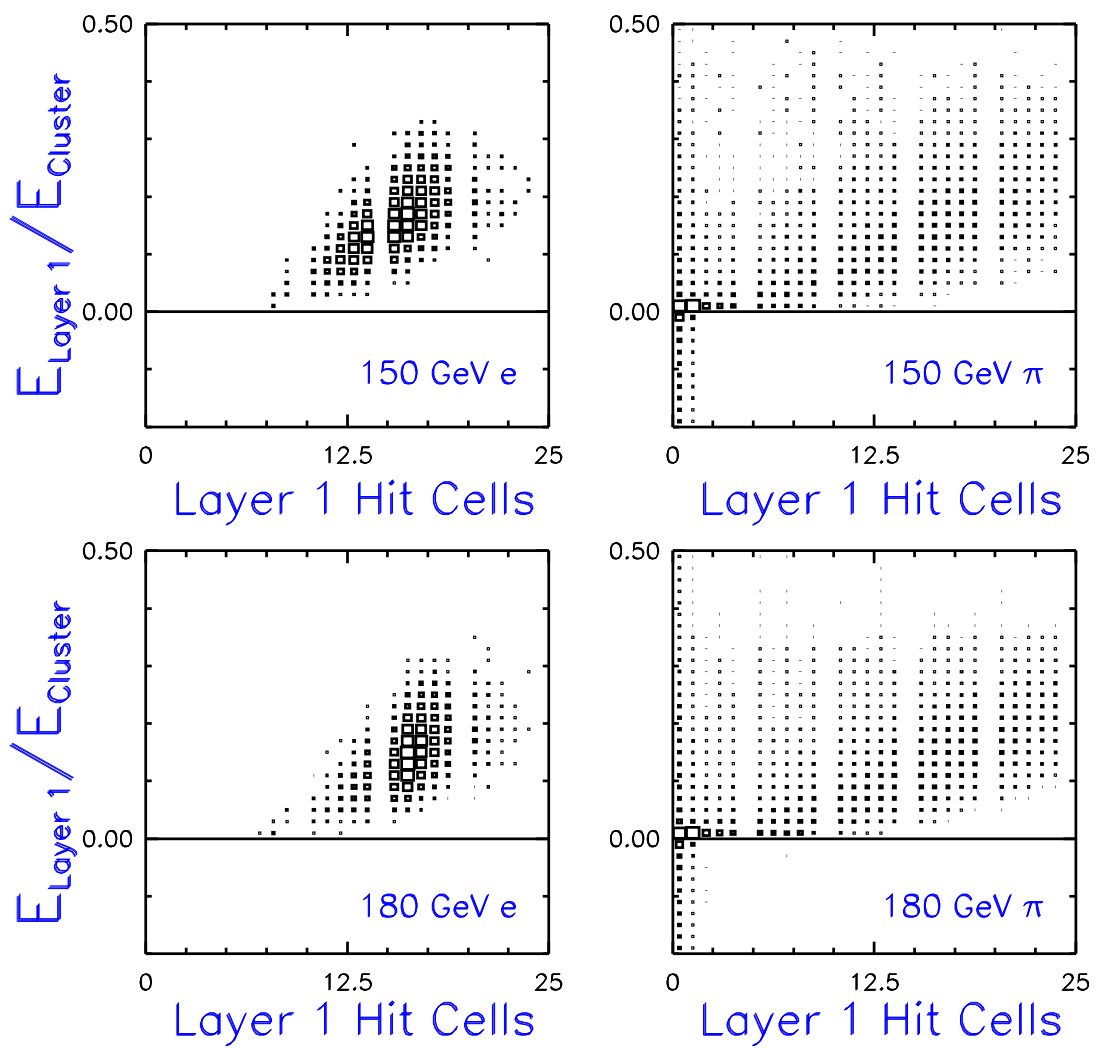
Figure 20: Number of Layer 1 hit cells vs $E_{Layer1}/E_{Cluster}$ 2d plots for 150GeV and 180GeV e and π samples.
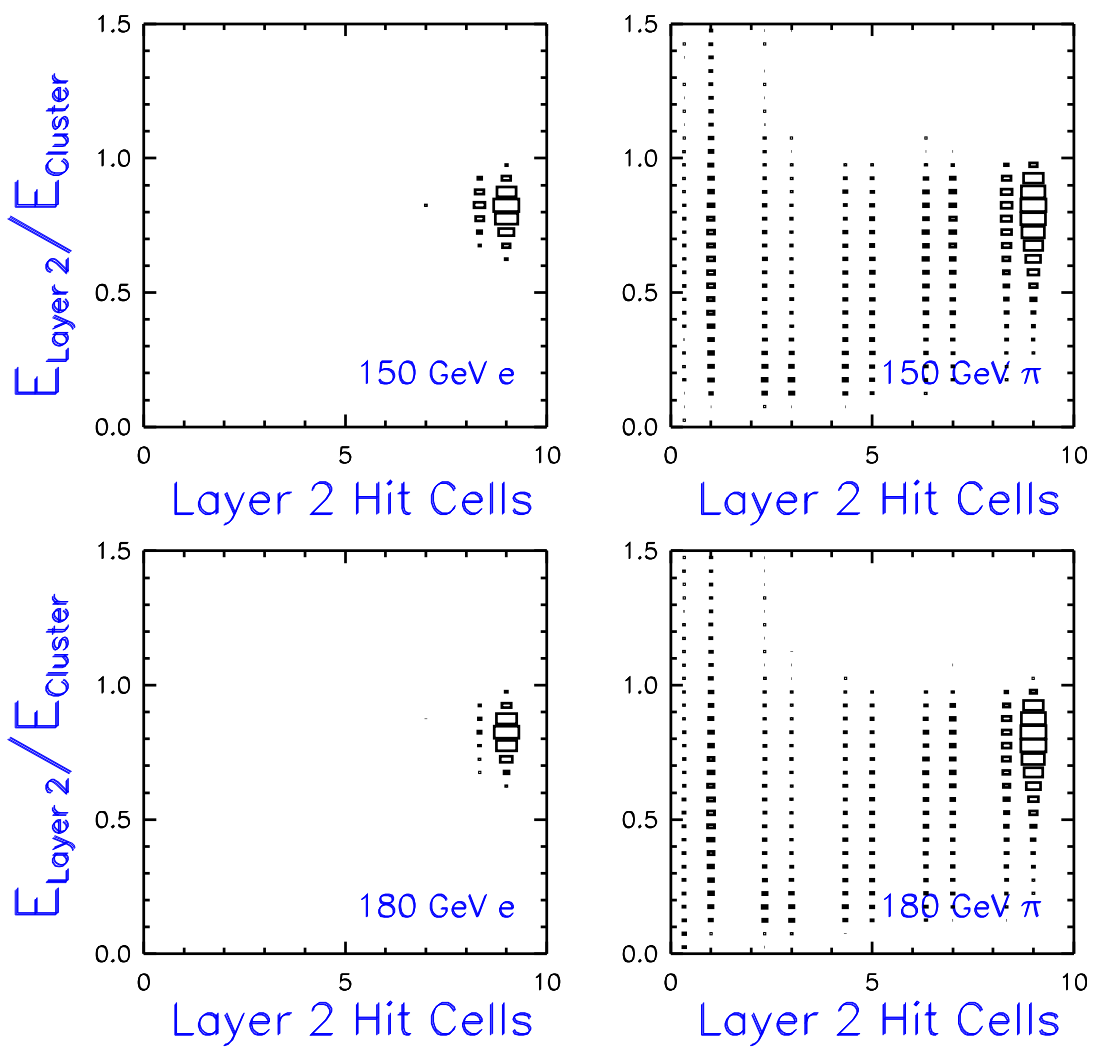
Figure 21: Number of Layer 2 hit cells vs $E_{Layer2}/E_{Cluster}$ 2d plots for 150GeV and 180GeV e and π samples.
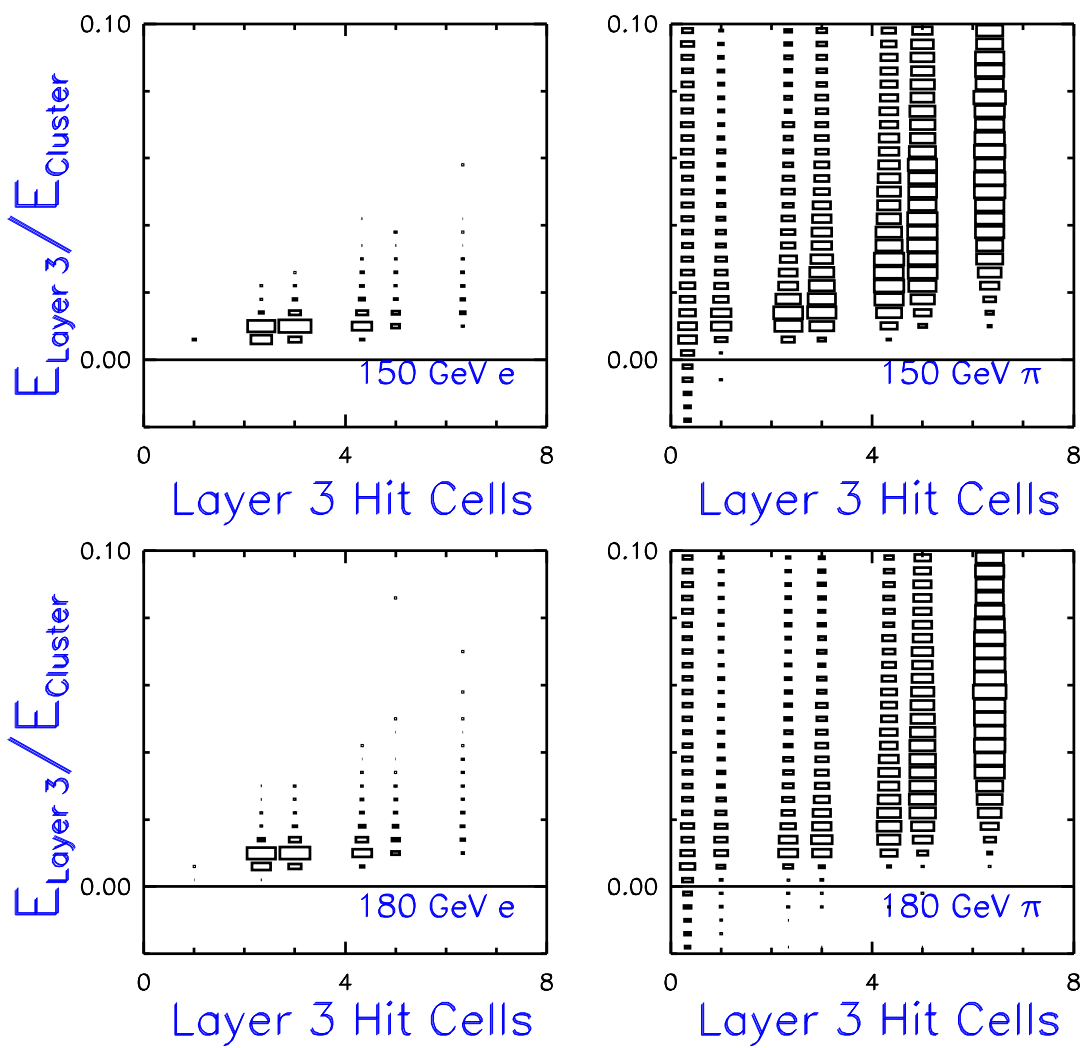
Figure 22: Number of Layer 3 hit cells vs $E_{Layer2}/E_{Cluster}$ 2d plots for 150GeV and 180GeV e and π samples.
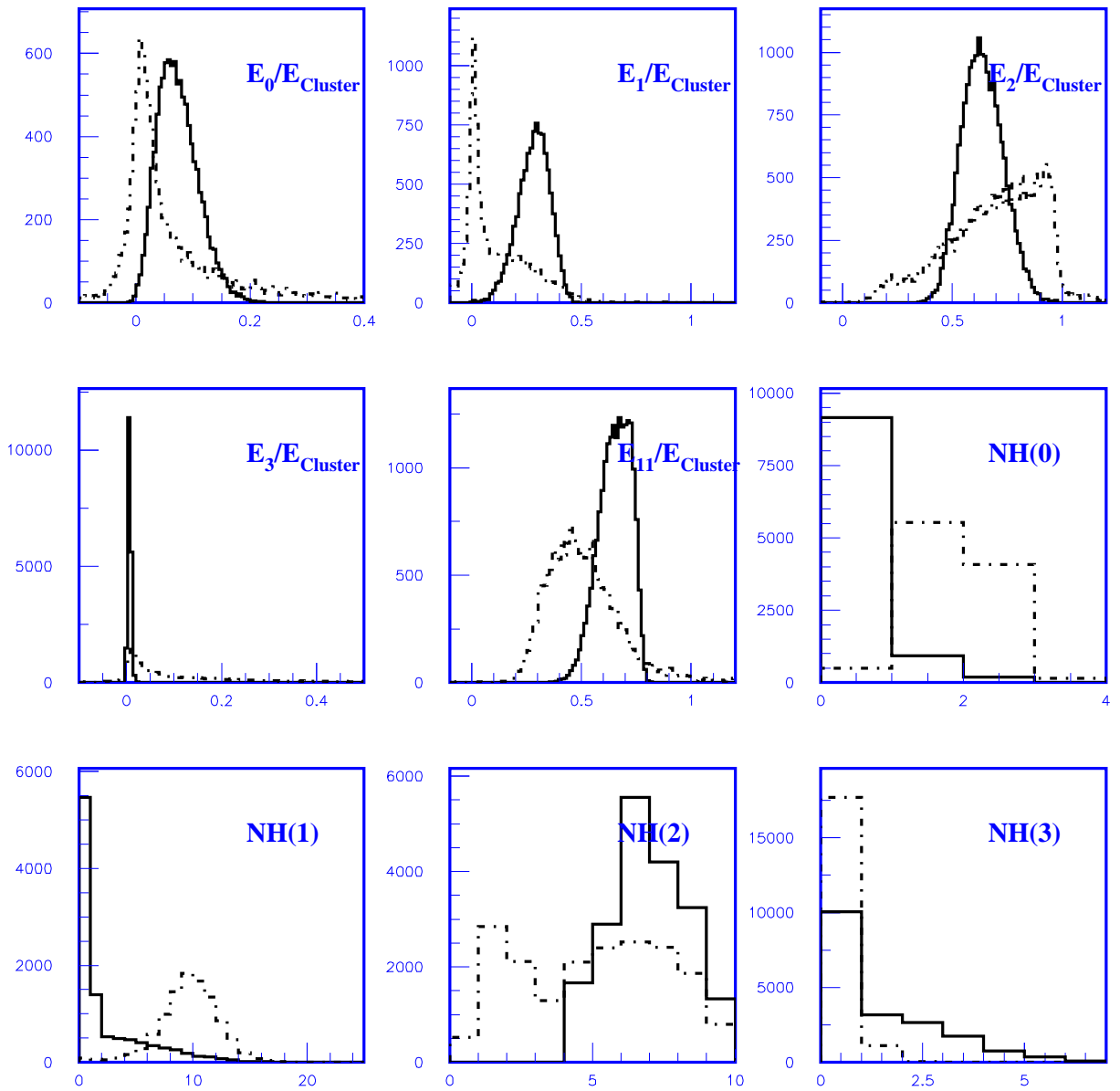
Figure 23: Simple cut and Neural network inputs of 20GeV electrons and pions
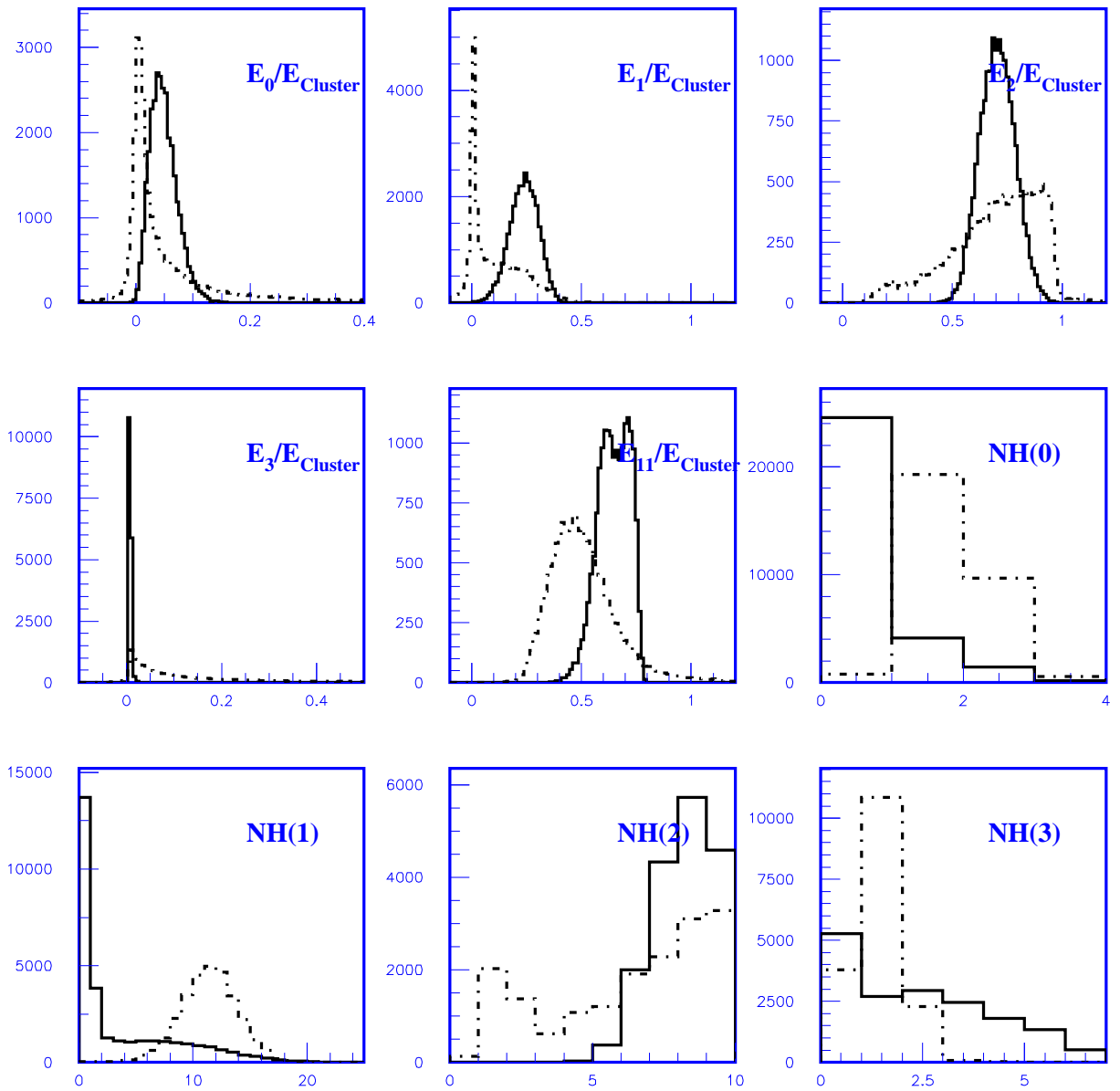
Figure 24: Simple cut and Neural network inputs of 40GeV electrons and pions
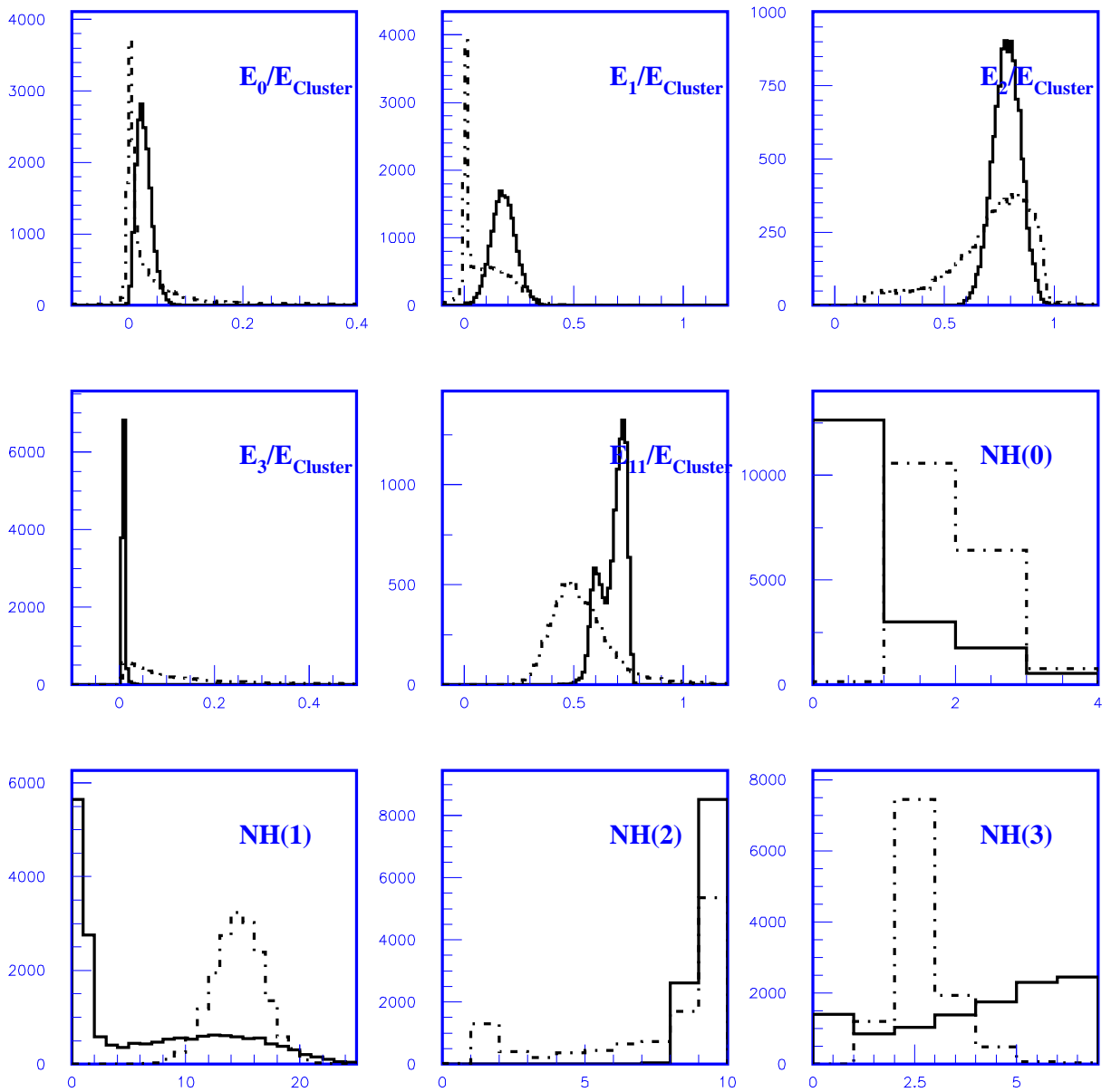
Figure 25: Simple cut and Neural network inputs of 100GeV electrons and pions
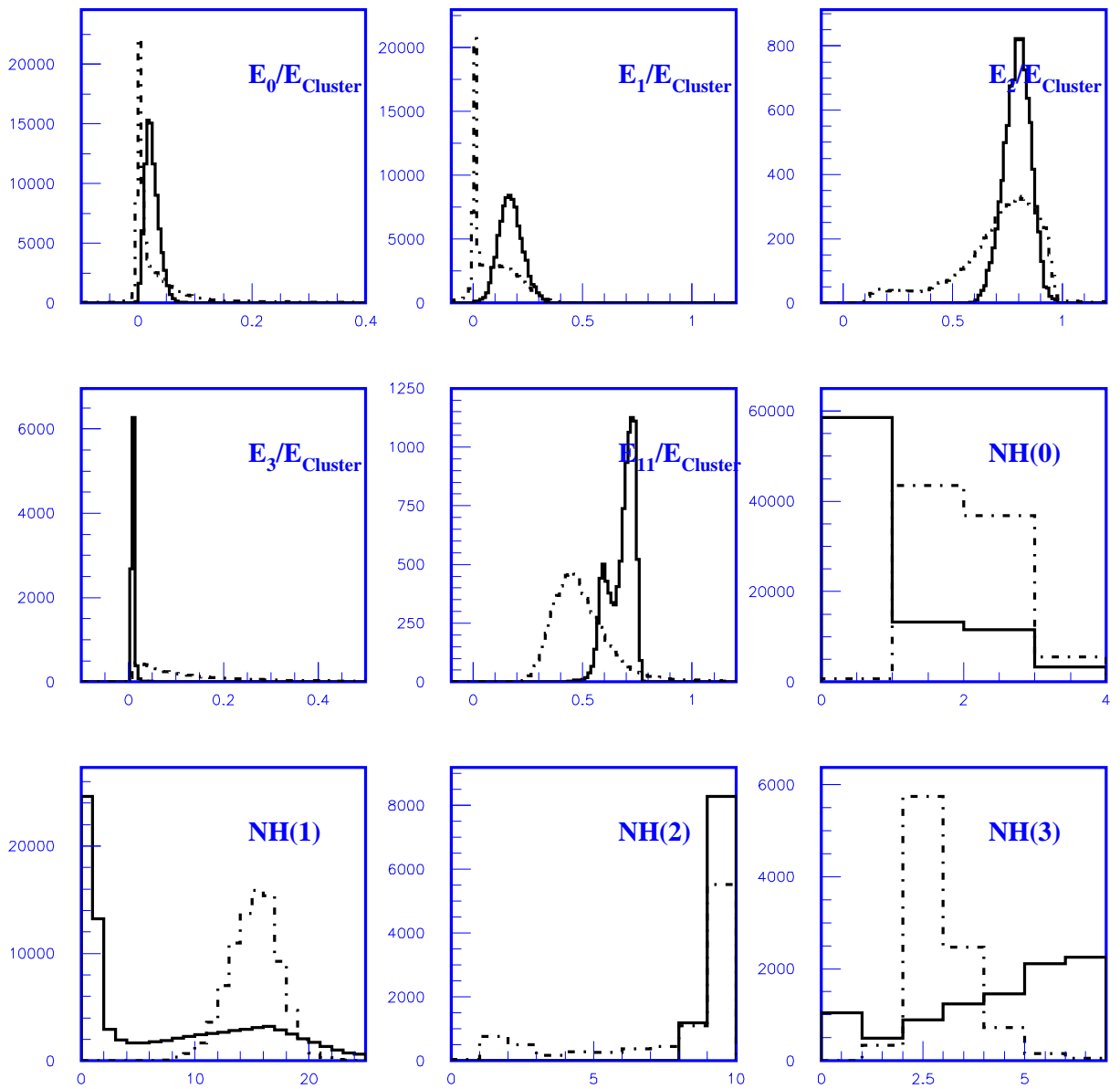
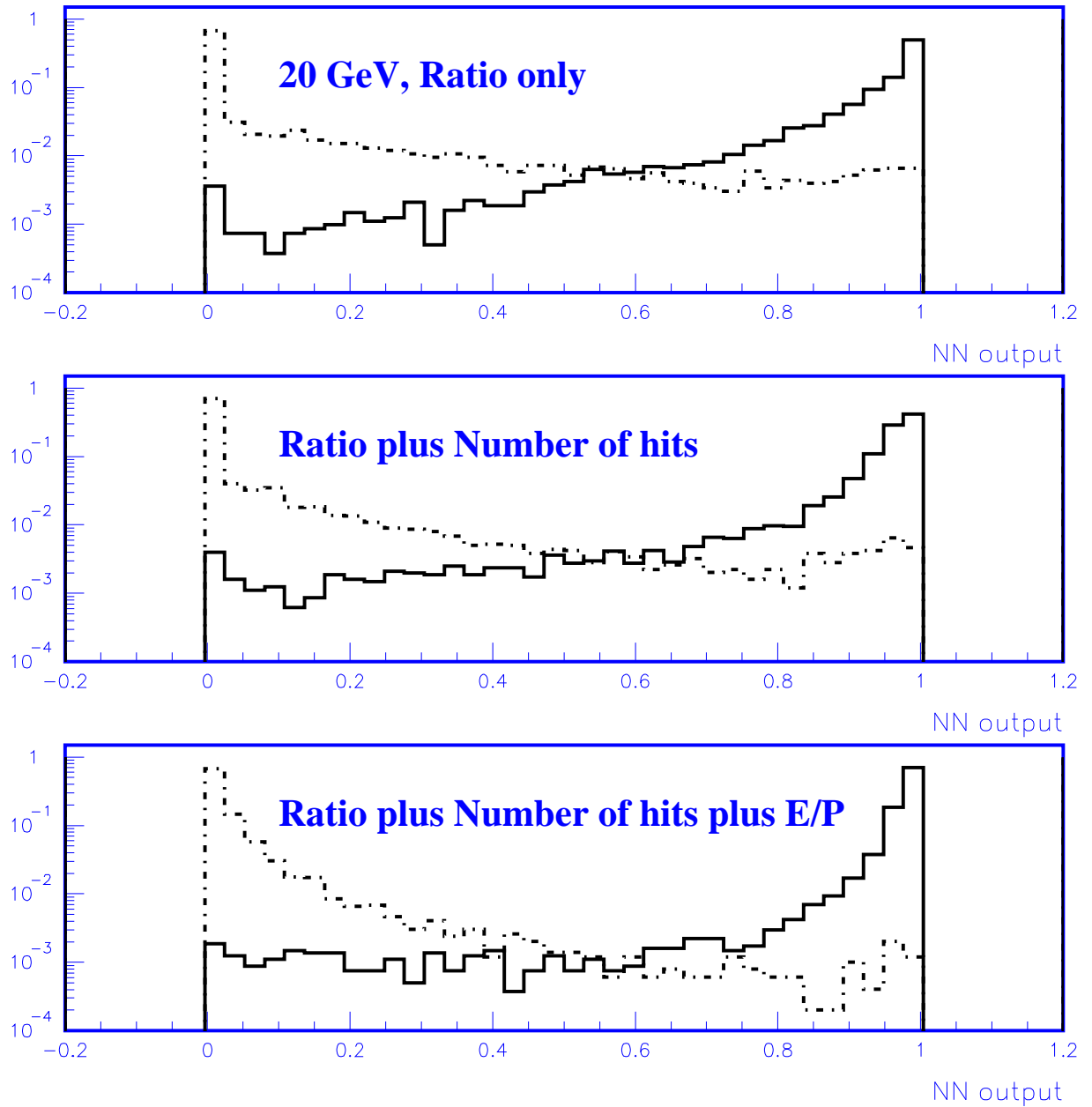Figure 26: Simple cut and Neural network inputs of 120GeV electrons and pions
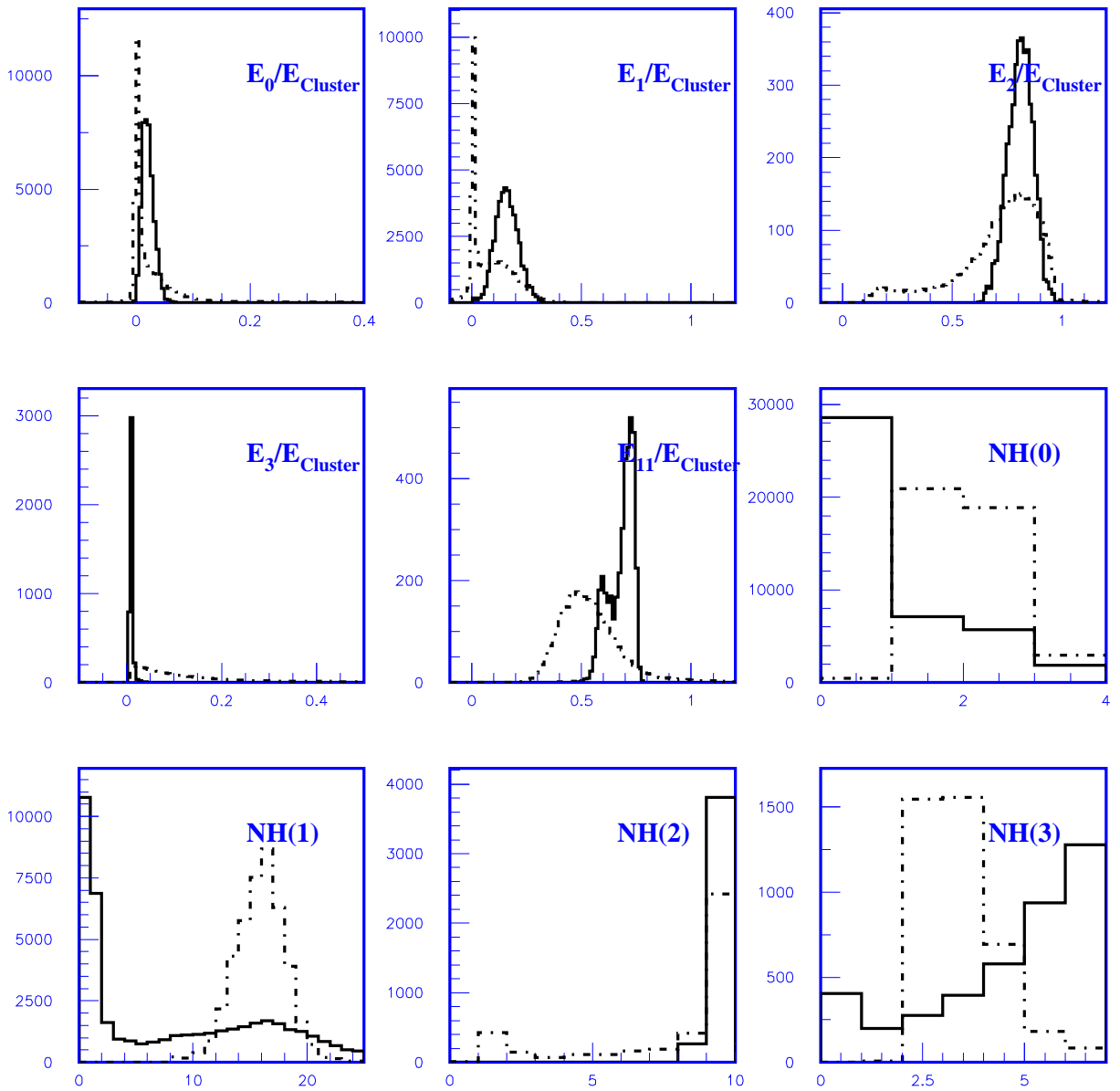
Figure 27: Simple cut and Neural network inputs of 150GeV electrons and pions
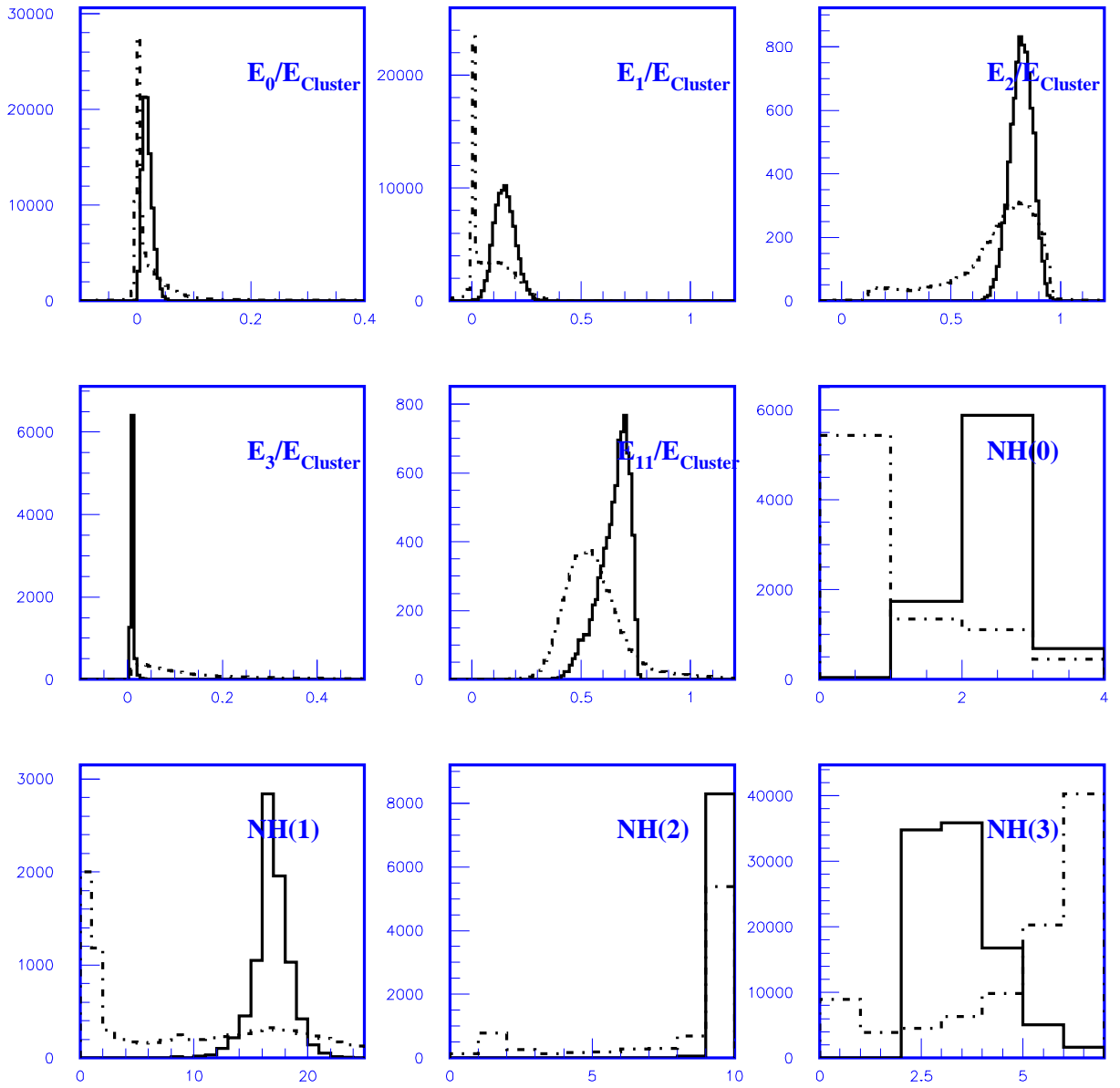
Figure 28: Simple cut and Neural network inputs of 180GeV electrons and pions

Figure 29: Neural network output of 20 GeV electron run and pion run. The dash line stand for the NN output for pions and the solid line is the output for electrons.
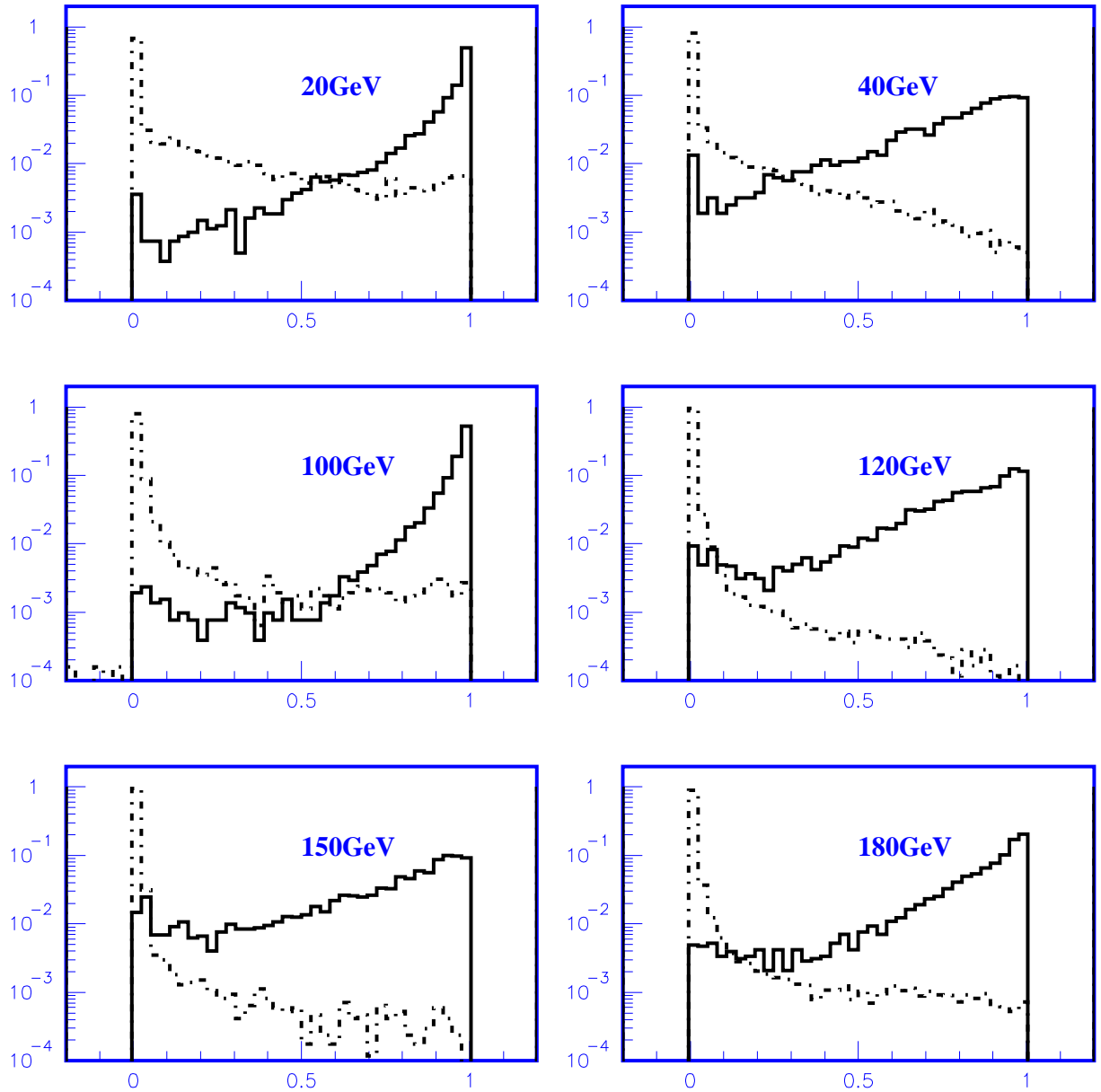
Figure 30: Neural network output for energies ratios only. The dash line stand for the NN output for pions and the solid line is the output for electrons.
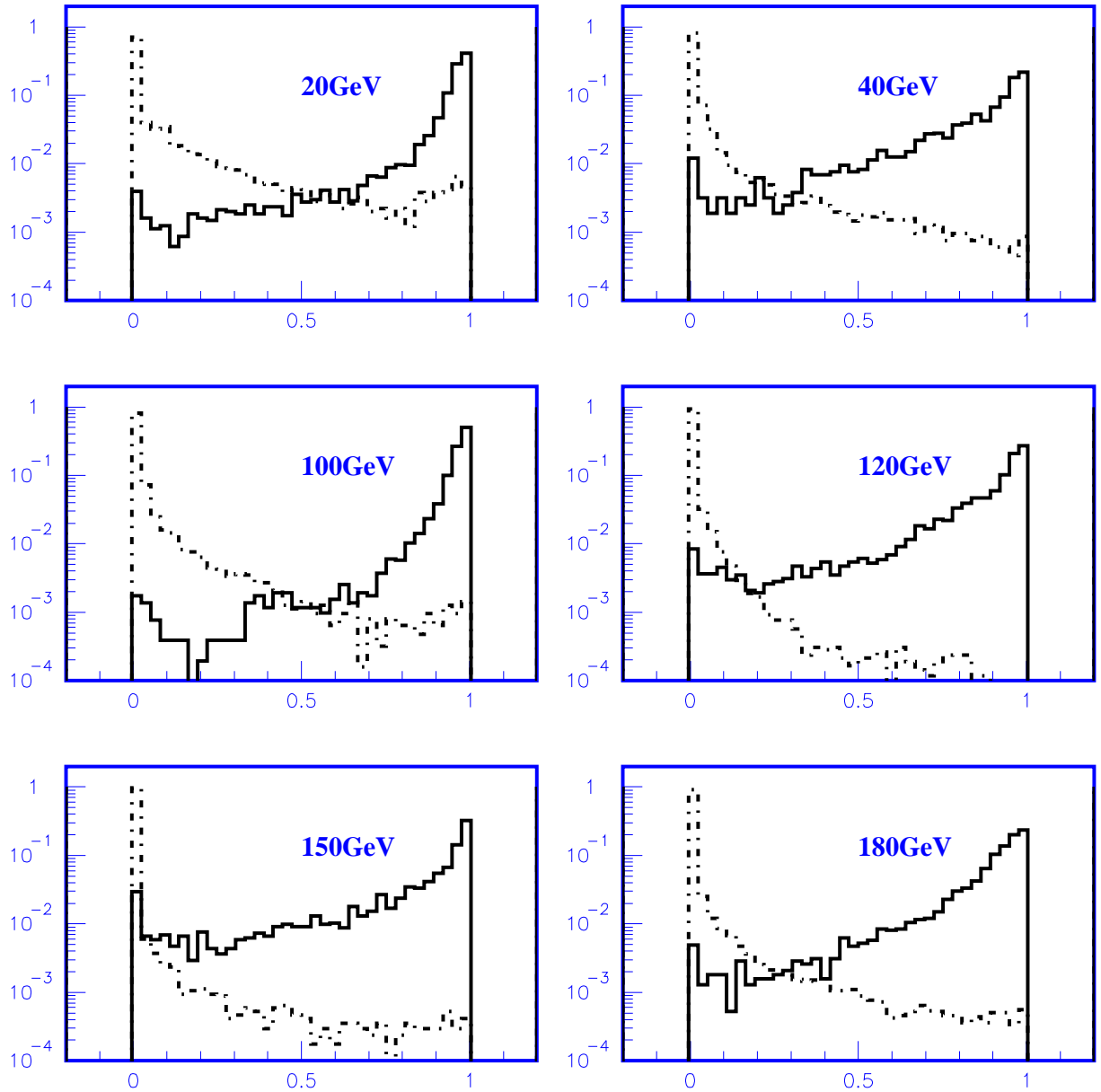
Figure 31: Neural network output for energies ratios plus the number of hits cells. The dash line stand for the NN output for pions and the solid line is the output for electrons.
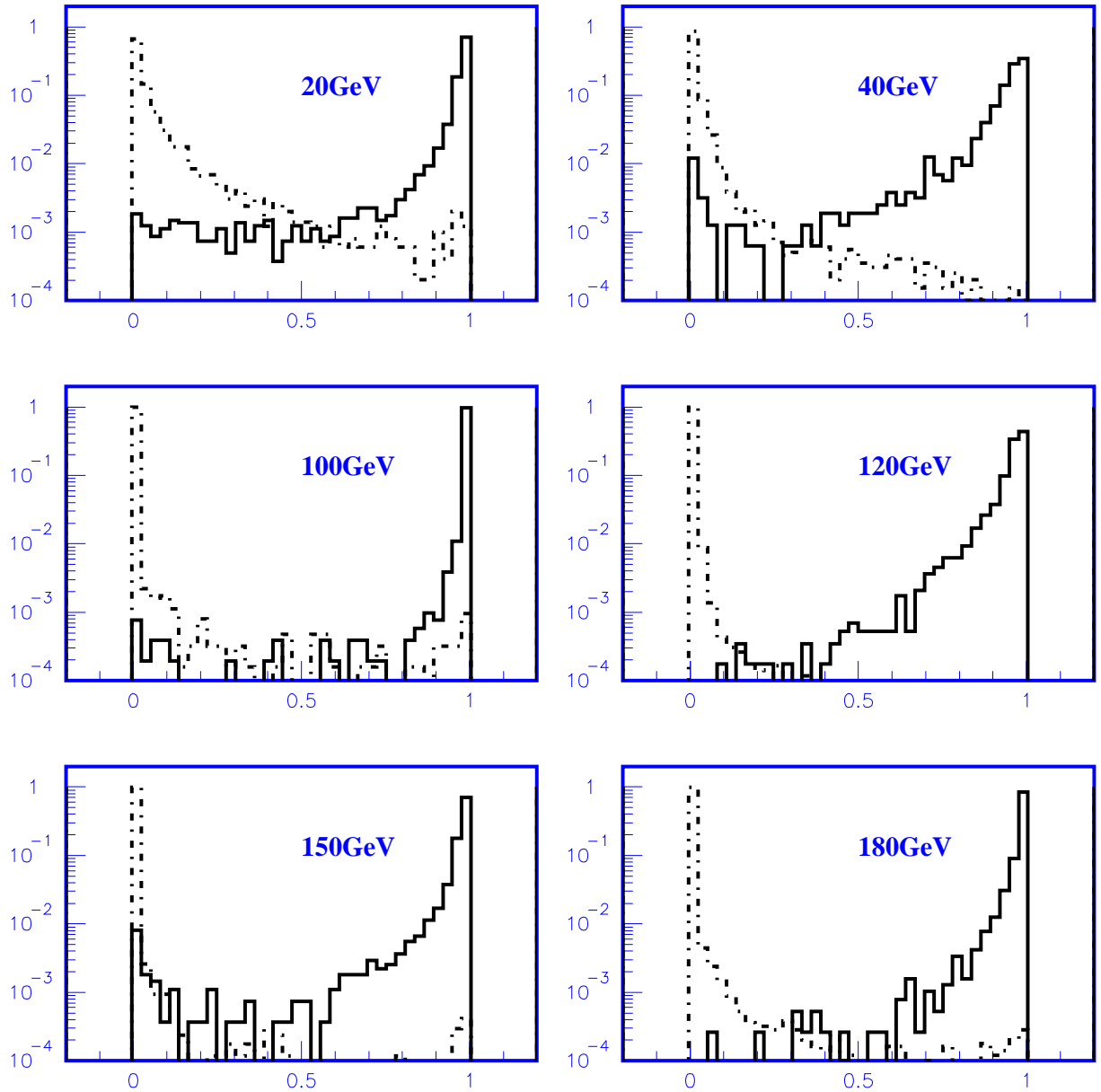
Figure 32: Neural network output for energies ratios plus the number of hits cells and the E/P. The dash line stand for the NN output for pions and the solid line is the output for electrons.